Bond behaviour of Steel Reinforced Polymer strengthening systems

Annalisa Napoli[a], Gianmarco de Felice[b], Stefano De Santis[b], Roberto Realfonzo[a]*

[a] University of Salerno, Department of Civil Engineering, Via Giovanni Paolo II 132, 84084 Fisciano (SA), Italy

[b] Roma Tre University, Department of Engineering, Via Vito Volterra 62, 00146 Rome, Italy

*Corresponding author

This is a post-peer-review, pre-copyedit version of an article published in Composite Structures

The final authenticated version is available online at:

http://dx.doi.org/10.1016/j.compstruct.2016.05.052

Bond behaviour of Steel Reinforced Polymer strengthening systems

Annalisa Napoli[1,a], Gianmarco de Felice[2,b], Stefano De Santis[2,c], Roberto Realfonzo[1,d,*]

[1] University of Salerno, Department of Civil Engineering. *Via Giovanni Paolo II 132, 84084 Fisciano (SA), Italy*
[2] Roma Tre University, Department of Engineering. *Via Vito Volterra 62, 00146 Rome, Italy.*

[a] annapoli@unisa.it, [b] gianmarco.defelice@uniroma3.it, [c] stefano.desantis@uniroma3.it, [d] rrealfonzo@unisa.it
* Corresponding author. T: +39 089 964085. F: +39 089 968739.

ABSTRACT

Steel Reinforced Polymer (SRP) systems, consisting of Ultra High Tensile Strength Steel cords and epoxy resin, are emerging as an effective and cost efficient solution for the externally bonded strengthening of structures. Their applications in civil engineering are more recent than those with Fibre Reinforced Polymers (FRP) employing carbon, glass or aramid textiles, and their mechanical properties still need to be deeply investigated. This paper presents an experimental study on SRP reinforcements comprising textiles with 4, 12 and 18 cord/in density. First, the mechanical properties of both textiles and SRP composites were derived through direct tensile tests. The shear bond behaviour, which is crucial for the effectiveness of most applications, was then investigated on strong and weak concrete, tuff, clay brick and brick masonry substrates, providing information on bond strength, failure mode, load-slip response and effective transfer length. Finally, test results and data available in the scientific literature are collected to calibrate the tuning coefficients for the estimate of the bond strength according to the design relationships provided by the Guidelines on FRP.

Keywords

Steel Reinforced Polymer (SRP); Bond; Concrete; Masonry; Experimental testing; Digital Image Correlation (DIC).

1. INTRODUCTION

Steel Reinforced Polymers (SRP) are an innovative class of composites for the externally bonded reinforcement of existing structures. They comprise unidirectional textiles made by twisting Ultra High Tensile Strength Steel (UHTSS) micro-wires to form cords. The first application of SRP in civil engineering was proposed in 2004 for the flexural strengthening of reinforced concrete beams [1]. Since then, a number of studies have been carried out to investigate the mechanical properties and durability of the steel textiles [2, 3], and the shear bond performance on concrete [4-7] and masonry [8-12] substrates. Experimental tests on medium and large scale specimens have shown that Steel Reinforced Polymer is an effective and cost efficient solution for the strengthening of reinforced concrete (see, amongst others [13-17]) and masonry [18-20] structures. Nevertheless, the most advanced standards, such as the Fib Bulletin 14 [21], the US guides ACI 440.2R-08 and ACI 440.7R-10 [22,23], and the Italian Guidelines CNR DT-200 R1/2013 [24], explicitly refer to Fibre Reinforced Polymers with carbon (CFRP), glass (GFRP) and aramid (AFRP) fibres (for which a more consolidated knowledge has already been developed), whereas steel textiles have been not included so far.

There are some differences related to manufacturing and nature of the steel textile with respect to carbon, glass and aramid ones: it is stiffer than glass and thicker than carbon and aramid, it is made of separated cords instead of being produced in compact fibre sheets, no bidirectional or multidirectional textiles are available. Nevertheless, the studies carried out to date (a state-of-the-art of which is provided in [25]) suggest that the mechanical behaviour of the SRP systems and of the structural elements reinforced with SRP can

well be considered comparable to that of the other FRP reinforcements. On the other hand, due to the lower number of experimental data with respect to CFRP, GFRP and AFRP applications, there are some aspects of SRP systems that would deserve a deeper examination for an improved understanding of their behaviour. At the scale of the structural element, the existing analytical relationships to estimate the effectiveness of SRP reinforcements should be either verified (possibly by recalibrating some coefficients) or developed for some specific applications, such as the confinement of columns and joints or the strengthening in bending and shear [26]. At a smaller scale, the SRP-to-substrate bond behaviour still presents some uncertainties, common to the design of most structural applications, that need to be tackled, namely:

(i) the debonding strength and the related failure mode for the main substrate typologies, such as concrete, masonry, and natural stone;
(ii) the effective transfer length, which is defined as that needed for the development of the full bond strength (i.e., that beyond which no strength increase is obtained);
(iii) the possibility of applying the design formula developed for the FRPs [24], or the need for calibrating specific tuning coefficients.

Due to the key role of the bond performance on the effectiveness of the external strengthening, a deeper investigation on these issues is needed before Steel Reinforced Polymer systems can be included with full rights in the standard codes for qualification and design.

This paper presents an experimental investigation carried out jointly by the University of Salerno and University of Roma Tre on SRP systems comprising three textiles with density of 4, 12 and 18 cord/in and a bi-component epoxy resin. The mechanical properties of both dry textiles and SRP composites were first derived through direct tensile tests. Then, the shear bond behaviour was investigated on high and low strength concrete, tuff, clay brick and brick masonry, in order to cover the main fields of application of externally bonded reinforcements. For each of them, the effective transfer length was evaluated through the analysis of the strain profile along the bonded area of the reinforcement. The influence of relevant parameters, such as the density of the textile, the bonded length, the mechanical properties of the substrate and its heterogeneity, was also explored. Finally, the results of the bond tests carried out in this study and those available in the scientific literature are collected to calibrate the average and the characteristic tuning coefficients for the estimate of the bond strength according to the design relationships of the Italian Guidelines CNR DT-200 [24].

2. MATERIALS AND EXPERIMENTAL PLAN

The SRP systems tested in this study comprise unidirectional textiles of Ultra High Tensile Strength Steel (UHTSS) cords, produced by Hardwire LLC [27]. Each cord has a cross section area (A_{cord}) of 0.538mm^2 and is made out of five wires with 0.11mm^2 area, three straight and two twisted around them at a short lay length (Fig. 1a). Wires are galvanized (coated with zinc) to provide protection against rusting, and are installed on a supporting glass mesh to ease storage and installation. Three different textiles were tested, with density of 4 (Fig. 1b), 12 (Fig. 1c) or 18 (Fig. 1d) cord/in, and labelled S4, S12 and S18, respectively. Table 1 collects their cord spacing, surface mass density (γ) and equivalent design thickness ($t = A_{cord} \cdot$density). Direct tensile tests were carried out to characterize both dry steel textiles and composite specimens. Steel Reinforced Polymer coupons were manufactured with a bi-component epoxy resin whose mean mechanical properties derived from direct tensile tests, performed by the manufacturer [28] on dog-boned specimens, are: tensile strength 17.9N/mm^2, Young's modulus 3.54kN/mm^2, and elongation at rupture 0.6%. The SRP specimens are identified by the letter R following the textile denomination (i.e., S4R, S12R and S18R). Finally, single lap bond tests were carried out to investigate the shear bond behaviour (in terms of strength, failure mode, and effective transfer length) on strong and weak concrete substrates at the University of Salerno and on tuff, clay brick and brick masonry substrates at University of Roma Tre.

3. TENSILE BEHAVIOUR OF STEEL TEXTILES AND SRP COMPOSITES

3.1. Specimens and testing setup

Direct tensile tests were carried out on dry textiles and SRP composites by using a Material Testing System

(MTS) load frame supplied with a 500kN hydraulic actuator. Textile specimens had 600mm length and were made out of 8 cords for S4, 24 cords for S12 and 35 cords for S18, while SRP specimens had 500mm length, about 2mm thickness, and comprised 5 cords for S4R, 15 for S12R and 25 cords for S18R series. Five tests were carried out for each series, corresponding to a total of 30 tensile tests. Aluminium tabs were glued on the ends of the specimens by means of a strong structural adhesive to ensure uniform stress distribution and prevent sliding in the gripping areas [29] (Fig. 2). Load was applied by the 500kN hydraulic actuator under displacement control at 0.01mm/s rate and recorded by a load cell with 0.2% accuracy and 0.01kN resolution. For both dry textile specimens and SRP coupons, stresses were evaluated by dividing the recorded load by the cross section area of the textile.

Three different displacement/strain measurement techniques were used. Global displacements were acquired by an LVDT integrated in the testing machine, recording the relative displacement from end plate to end plate with 0.05% accuracy and 1μm resolution. The corresponding average strains were derived as the recorded displacement divided by the initial distance between the clamping wedges. Local strains were detected by an MTS extensometer having 50mm gage length, +25/-5mm range, 0.18% accuracy and 10με resolution, placed in the middle of the specimen (Fig. 2a). Finally, in tests on SRP coupons, the displacement field was measured by means of Digital Image Correlation (DIC). To apply DIC technique, the specimen was prepared by realizing a speckle pattern made of randomly distributed black dots on a white background (Fig. 1b). During test execution, photographs were taken with a digital camera, positioned on a stiff frame at 1.20m from the specimen, taking care of ensuring correct alignment to avoid image distortions. Two LED spotlights were used to keep stable and even illumination. Pictures had 3888×2592 pixels, which corresponds to a pixel size of 0.11mm. After post-processing with sub-pixel interpolation algorithms [30], the resulting displacement resolution was <0.01mm. Within picture analysis, two points were selected on the surface of the specimen and their relative displacements were measured and divided by their initial distance to derive strains. The comparison between the LVDT integrated in the testing machine, the extensometer and the DIC allows for the mutual validation of both the three techniques and the strain data, as shown in the stress-strains experimental responses referring to one specimen of the S4R series (Fig. 3a), one of the S12R series (Fig. 3c) and one of the S18R series (Fig. 3e), taken as examples. The agreement between global (LVDT) and local (extensometer, DIC) measurements also proves that no sliding occurred in the gripping areas.

3.2. Test results

Figs. 3a,c,e show the stress-strain curves obtained from all tensile tests performed on dry textile specimens and SRP composites for S4R, S12R and S18R series, respectively. In these plots, strains are derived from the recordings of the LVDT integrated in the testing machine. These strain data agree with those obtained with different displacement/strain measurements (i.e., extensometer, DIC), as shown in Figs. 3b,d,f related to one specimen per series taken as sake of example.

The response of dry textile specimens is characterized by an initial linear elastic phase, followed by a nonlinear phase. The monotonic load increase indicates that failure occurs by the nearly simultaneous rupture of the cords (Fig. 3 would otherwise show load drops at premature cord failure). Table 2 lists average tensile strength (f_t), Young's modulus (E_t), computed between 10% and 50% of f_t (as recommended for FRPs by [31]), maximum attainable load per unit width (F_t) and strain corresponding to the peak stress (ε_t). The Coefficients of Variation (CV), always very low, are indicated in round brackets. Due to the larger number of cords and the higher stiffness of the specimens made of denser textiles (S12 and S18), it is more difficult to ensure that all the cords are evenly loaded. This may anticipate the rupture, as indicated by the slightly lower values of both the strength (3065-3085N/mm^2) and the peak strain (2.09%) if compared to S4 (3191N/mm^2 and 2.19%). Given the similar tensile strength (in terms of stress), the maximum load per unit width highly grows with the increase of the cord density. The Young's modulus is about 182kN/mm^2 for all the densities, in agreement with previous experimental studies performed on analogous textiles [15, 29, 32]. Table 2 also reports the main results of tensile tests on SRP specimens. No significant difference is found with dry textile in terms of tensile strength, which only relies on the steel cords. On the other hand, the stiffening effect of the resin matrix produces both a slight reduction of the peak strain and an increase of the secant Young's modulus (evaluated between $0.1f_t$ and $0.5f_t$, as for dry textiles). The lower is the density of the cords the larger is the relative amount of resin in the cross section of the specimen, and the resulting stiffness mismatch between dry textiles and SRP composites (note that stresses are always referred to the cross-section area of the dry textile). For the same reason, the slope reduction associated to some damage development in the matrix is detectable in S4R specimens and not in S12R and S18R. The initial Young's modulus E_f (evaluated between $0.05f_t$ and $0.1f_t$) could be estimated, under the assumptions (valid until the

resin is undamaged) of linear elastic behaviour of the materials and perfect steel-matrix bond, as $E_t(1+\beta)$, with $\beta=E_mA_m/(E_tA_s)$, E_m and E_t being the Young's modulus of the resin and of the dry textile (as said before), and A_m and A_s the respective cross section areas. The value of the β coefficient (in which A_s is at the denominator) confirms the experimental trend.

4. SRP-TO-SUBSTRATE SHEAR BOND BEHAVIOUR

4.1. Testing setup and plan of shear bond tests

Shear bond tests were carried out on the three SRP systems (comprising steel textiles with 4, 12 and 18 cord/in) on the following substrates:

- Concrete blocks, measuring 400mm×200mm×150mm. Two grades of concrete were considered such as a high strength concrete (labelled as HSC) and a low strength concrete (LSC);
- Tuff units (TU), measuring 120mm×245mm×110mm;
- Clay bricks (CB), measuring 120mm×250mm×55mm;
- Prisms of brick masonry (BM), manufactured with the same clay bricks, and hydraulic lime mortar (classified as M5 according to [33] with a conventional compressive strength of 5N/mm^2). Prisms had 120mm×120mm cross section and were made of four (or five, depending on the bonded length of the SRP) half bricks and three (or four) 10mm thick mortar joints (Fig. 4). The incidence of deep mortar joints (dug with respect to the surface of the brick of about 5mm) was also investigated, to reproduce the characteristic of the surface in some real applications on existing masonry structures (in this case the substrate is labelled BMJ).

Table 3 collects the main mechanical properties of the substrates, such as compressive (f_{cs}) and tensile (f_{ts}) strength and Young's modulus (E_{sub}). The clay brick has an anisotropic behaviour, since its compressive strength is 14.8N/mm^2 if measured in the direction normal to the bed face ($\perp$) and 18.5N/mm^2 if measured in the direction parallel (//) to the bed face (normal to the side) [12]. For tuff and clay brick, the normalized compressive strength values, evaluated according to EN 772-1:2011 standard [34] are indicated. For masonry prisms the compressive strength and the Young's modulus were derived through compression tests [12].
SRP reinforcements were bonded to the substrates by following a standard wet lay-up procedure. One layer of textile was placed in the centre line of one side of the substrate, after having cleaned its surface with compressed hair. A roller was used to ensure proper impregnation of the resin both in the substrate and through the voids of the textile. Due to the specific characteristics of the setups used for shear bond tests, the width of the bonded area was 100mm for concrete substrates and 50mm for tuff, brick, and masonry. Different bonded lengths (L_b) were tested, such as 150mm and 300mm on concrete substrates, 200mm on tuff and brick, and both 200mm and 280mm on brickwork. The specimen series were labelled by indicating the strengthening system, the substrate and the bonded length. For instance, the group of specimens comprising the textile with 12 cord/in bonded to the high strength concrete for a length of 150mm are named S12R-HSC-150.
Two single-lap setups were used by University of Salerno for shear bond tests on concrete substrates (Fig. 5a) and by University of Roma Tre for test on masonry substrates (Fig. 5b). In both cases, the specimen was placed and kept fixed by a stiff supporting steel frame, and the unbonded textile was clamped in the wedges of the testing machine and pulled to apply the shear load at the SRP-to-substrate interface, taking care of ensuring alignment. Test were performed under displacement control at a rate of 0.01mm/s for concrete and 0.003mm/s for masonry substrates.
The following sections describe the shear bond tests on concrete and masonry substrates and report the main results, such as debonding load and corresponding slip, stress in the textile at failure and corresponding exploitation ratio of textile tensile strength, load-slip curves, failure modes, and strain profiles.

4.2. Concrete substrates

In the case of concrete substrates, tests were carried out with a Schenck load frame provided with a hydraulic actuator with 630kN capacity. Forces were recorded by a load cell integrated in the testing machine and also, as a further control, by an external 200kN load cell placed below the steel base plate and restrained to the lower cylindrical element of the testing machine (Fig. 5a).

The relative displacement (slip) between SRP reinforcement and substrates at the loaded end (first bonded section on the side of load application) was either measured directly or calculated indirectly. The direct method made use of a laser displacement transducer with 100mm full-stroke (f.s.) and 0.06% f.s. accuracy. The indirect method consisted in calculating the slip as the global displacement measured by the LVDT integrated in the testing machine minus the elastic elongation of the unbonded portion of the steel textile (about 140mm). As a further control, other two laser sensors were used to monitor the possible slip at the unloaded end of the SRP tape and at the gripping system. Finally, a number of strain gauges (with 20mm gauge length, 2.12 gauge factor and 120Ω resistance) were bonded to the SRP tape to measure the axial strains and derive the strain profiles.

In total, 19 shear bond tests were carried out on the three SRP systems (S4R, S12R and S18R) bonded to concrete substrates, 11 of which on high strength concrete (HSC) and 8 on low strength concrete (LSC). For each series (group of specimens nominally identical) Table 4 collects the main data, such as: bonded length (L_b) and width (b_f), series label and number of tested specimens (N), maximum load ($F_{b,i}$) and corresponding slip (s_i) of the individual specimens and the corresponding average values F_b and s (with CV in round brackets). The stress is calculated as $\sigma_b=F_b/(A_f)$, A_f being the area of the textile calculated as the product of design thickness (t) and width (100mm in this case). The corresponding exploitation ratio (defined as the ratio between the debonding stress and the average value of the tensile strength of the textile derived from experimental tests, Table 2) is calculated as $\eta=\sigma_b/f_t$. Finally, the maximum load per unit width is derived as $F_b^* = F_b / (b_f \sqrt{k_b})$, b_f being the width of the reinforcement strip and $k_b = \sqrt{(2 - b_f / b)/(1 + b_f / b)}$ a geometrical corrective coefficient that accounts for width effects (i.e., to the fact that the portion of substrate involved in the debonding is larger than the composite strip due to the penetration of the epoxy resin), defined according to the Italian Guidelines CNR DT-200 [24]. In this case, since b=200mm and b_f=100mm, k_b=1. The maximum load per unit width is particularly important for engineering design purposes as it rules the strengthening layout (width and spacing between SRP strips) and, together with the exploitation ratio, may be assumed as a parameter for comparing the efficiency of different reinforcement systems.

The slip values provided in Table 4 are derived via indirect method, except for the series S4R-HSC-300, for which the slip was measured by the laser transducer placed at the loaded end of the SRP tape (in the table these slip values are in italics). However, when both direct and indirect measurements of the slip were available, a rather good matching was verified as confirmed by the load-slip comparison curves depicted in Figs. 6a and 6b for the sake of example and related to one specimen of the series S12R-HSC-300 and S12R-HSC-150, respectively. More specifically, the two methods provide comparable results, with a very good agreement until the load is about 50% F_b, and a certain mismatch arising only in some specimens due to the development of cracks in the substrate, making the recordings of the laser transducers unreliable at high load values (Fig. 6b). Finally, due to the lack of both the considered measures, no slip data is available for the series S4R-LSC-300 and for one specimen of the series S18R-LSC-300.

Test results provide the following indications about the incidence on the bond strength of (i) bonded length (L_b=150mm/L_b=300mm), (ii) concrete grade (high/low strength), and (iii) density of the steel textile in the SRP reinforcement (4/12/18 cord/in):

(i) for a given concrete grade and textile density, the shear bond strength increases very slightly with the bond length (as an example, compare the series: S12R-LSC-150 and S12R-LSC-300; S18R-LSC-150 and S18R-LSC-300; S12R-HSC-150 and S12R-HSC-300). This suggests that either the effective transfer length is slightly longer than 150mm, or the longer is the bonded length the higher is the probability of coming over a portion of concrete that locally has a higher surface strength;

(ii) the different grade of concrete substrate does not significantly affect the shear bond strength, especially for the reinforcements comprising the denser textiles (S12R and S18R), for which the increase is in the order of 5-7%. Differently, with S4R the difference is about 24%;

(iii) for a given bond length and concrete grade, the debonding load (F_b) increases with the textile density (as an example, compare the series: S12R-LSC-150 and S18R-LSC-150; S12R-HSC-150 and S18R-HSC-150; S4R-LSC-300, S12R-LSC-300 and S18R-LSC-300; S4R-HSC-300 and S12R-HSC-300), which is likely to be related to a relatively longer effective bond length of the denser (and therefore stiffer) textiles. Such variation, however, is less than proportional with the design thickness, as revealed by the values of the maximum load per unit width (F_b*), which vary from 207-256kN/m (S4) to 268-307kN/m (S12), to 289-326kN/m (S18). Finally, the exploitation ratio of the tensile strength of the textile strongly reduces passing from S4R (η=77-96%), to S12R (η=34-39%), and to S18R (η=21-24%) systems.

Figs. 7 and 8 show the load-slip response curves for some specimens; as for Table 4, the plotted slip data are derived through indirect measurement. In particular, the graphs in Figs. 7a,b show, for a given textile density (i.e., 12 cord/in, system S12R) and concrete strength (HSC or LSC), the influence of the bonded length on the bond behavior. The load-slip response of specimens with longer bonded length (see series S12R-HSC-300 and S12R-LSC-300), displays repeated load drops at relatively high load levels (beyond 60-70% F_b, as a general trend), due to the progressive debonding of the SRP laminate from the substrate, associated to an extended capability of transferring the load. Debonding activates at the loaded end of the bonded reinforcement and then propagates towards the free end, up to the complete SRP detachment. The longer is the bonded length, the larger is the ultimate slip at which complete detachment occurs. Fig. 7c shows the incidence on the load-slip curve of both the substrate strength and the length of bonded reinforcement for S18R systems. For the same value (L_b=150mm) a higher concrete strength slightly affects the response, as it only implies the occurrence of a few load drops (absent in the case of LSC). Conversely, the higher load level achieved by increasing the length of the bonded reinforcement (see series S18R-LSC-300) seems to confirm that the denser textile needs an effective bond length slightly greater than 150mm.

The dependence of the textile density on the load-slip behavior is shown in Figs. 8a,b for a given concrete strength (LSC) and bonded length (L_b=150mm or L_b=300mm). This comparison confirms that the influence of the denser textile for any value of L_b is rather poor. Conversely, disregarding the textile density, the bonded length strongly affects the bond behaviour, since a longer L_b implies both a larger deformability and higher slip values at failure.

In all tests, failure occurred by cohesive debonding within the substrate, with the removal of a 2-3mm thick layer of concrete (Fig. 9a), as typically happens also in carbon, glass or aramid FRP reinforcements (see, amongst others [35-38]).

The axial strain distribution in the reinforcement is plotted in Figs. 10-11 for some representative specimens, at different load levels, ranging from 10% to 100% F_b. Strain values were recorded by resistive strain gauges glued on the SRP tape, with a greater concentration in the first half of the bonded length. The strain profiles recorded on specimen #2 of S4R-LSC-300 series are shown in Fig. 10. The first 60mm of the composite were involved in the load transfer up to a load of 80%F_b. This stress transfer zone then increased up to about 120mm at 90%F_b and 100%F_b. At this stage, a change in the concavity of the profiles can also be observed, which indicates that the debonding process has activated and moves away from the loaded end. The strain gauges glued at 150mm, 195mm, 240mm and 285mm did not record any significant strain values, suggesting an effective bond length of 130-150mm for S4R on LSC substrate. No strain data are available for this composite on HSC.

The graphs in Figs. 11a,b depict the strain distribution of two specimens having the same substrate (HSC) and bonded length (L_b=150mm) but different textile density (12cord/in in Fig. 11a and 18cord/in Fig. 11b). Relatively high strain values were achieved only in the first 60mm of the laminate starting from the loaded end for most of the loading process, while the remaining portion of the textile was engaged only when approaching the peak load. The maximum strains recorded by the gauges closest to the loaded end are 0.58% for S12R (Fig. 11a) and 0.40% for S18R (Fig. 11b). The ratio 5.8/4=1.45 approximately coincides with that between the areas of the two textiles S18 and S12 (1.5).

The graphs in Figs. 11c,d refer to S12R and S18R reinforcements bonded for a length L_b=150mm, as in Figs. 11a,b, but to the low strength concrete (LSC) substrate. The maximum strains achieved in the textiles approximately equal those recorded on high strength concrete (note that the maximum loads do not differ significantly), but in this case a longer portion of the SRP tape was engaged already at 50%-60% F_b, indicating that a longer effective bond length is associated to the more deformable substrate.

Finally, the strain profiles recorded on specimens with L_b=300mm and low strength concrete are plotted in Fig. 11e (SRP with S12 textile) and Fig. 11f (SRP with S18 textile). With respect to the previous cases with L_b=150mm, a similar maximum strain value was reached in S12R reinforcement (0.52%, Fig. 11e), while a slightly higher strain (0.50%) was recorded by the strain gauge closest to the loaded end on the S18R reinforcement (Fig. 11f), due to the increase of the maximum load (from 29.5kN to 35.1kN). In every instance, the strain recorded at failure by the strain gauge closest to the loaded end of the bonded area agrees with the theoretical value $F_b/(A_fE_t)$, also depicted in the plots of Fig. 10, which, clearly, is an average value over the width of the reinforcement. The strain profiles of SRP reinforcements bonded for a longer length clearly exhibit a change in the concavity at high load values (90%-100% F_b), related to the propagation of the debonding process along the bonded area of the SRP tape, which was not detected with the shorter bonded length. These graphs indicate that for the SRP systems comprising S12 and S18 textiles the effective bond length is about 150-170mm, which is the distance from the loaded end where the strain goes to zero when the concavity of the strain profiles changes. This length is slightly higher than that suggested by the strain

profiles in Fig. 10, referred to a reinforcement with S4 textile (130-150mm), characterized by a lower axial stiffness.

4.3. Masonry substrates

Shear bond tests on masonry substrates were carried out with the same MTS load frame used for the direct tensile tests; the applied load was recorded by the load cell integrated in the testing machine (like in tensile tests). The slip at the loaded end of the SRP reinforcement was recorded by two LVDTs having ±5mm f.s., 0.5% f.s. accuracy, and <10μm resolution. Digital Image Correlation (DIC) was also used to record the displacement field on the surface of the specimen and validate the slip measurement provided by the LVDTs. With DIC, the slip was derived as the relative displacement between two points, one on the substrate and one on the unbonded portion of the steel textile (Fig. 5b). Finally, an extensometer was placed on the unbonded textile to acquire a further strain measure.

Three shear bond tests were performed on tuff substrate, five on clay brick and nine on brickwork, six of which on prisms with plain joints and three on prisms with deep joints. In all cases, the width of the bonded area was b_f=50mm and the bonded length was L_b=200mm, with the only exception of one series on brickwork with plain joints, for which a longer bonded length (L_b=280mm) was also investigated.

Table 5 collects the bonded length (L_b) and width (b_f), series label and number of tested specimens (N), maximum load ($F_{b,i}$) and corresponding slip ($s_{,i}$) of the individual specimens and the corresponding average values F_b and s (with CV in round brackets), the stress in the textile σ_b, the exploitation ratio η and the maximum load per unit width F_b^*. In the case of masonry, the geometrical corrective coefficient is defined as $k_b = \sqrt{(3-b_f/b)/(1+b_f/b)}$ [24] and is equal to 1.35 (b=120mm and b_f=50mm,).

Failure occurred by cohesive debonding within the substrate on tuff (Fig. 9b), clay brick (Fig. 9c) and brickwork (Fig, 9d) substrates. Like in tests on concrete, this failure mode coincides with that occurring with FRP reinforcements comprising carbon [39], glass [40] and also basalt [11] fibres. The maximum load of S12R reinforcements bonded to clay brick was 7.8kN, while a debonding strength of 8.6kN (about 10% higher) was found in tests on masonry prisms with plain joints. Such an increase, already observed in previous studies [12], is likely to be related to the higher strength of the brick in the transverse direction and to an interlocking effect caused by the presence of the mortar joints. This latter was further increased by the deep joints, resulting in a particularly irregular failure surface (Fig. 9d) and in a significantly higher bond capacity (11.5kN on average). Finally, the increase of bonded length (from L_b=200mm to L_b=280) does not significantly affect the bond strength (compare the series S12R-BM-200 and S12R-BM-280 in Table 5). The difference is in the order of 4%, which is within the scatter of experimental data (CV=5-9%), and suggests that the effective bond length on this substrate is shorter than 200mm. According to the large variation of the bond strength exhibited on the investigated substrates, the maximum load per unit width varied from 55kN/m (on tuff) to 195kN/m (on brickwork with deep joints), as listed in Table 5. The exploitation ratios range from 9.7% on tuff (the weakest substrate) to 19.6% on clay brick and about 22% on brickwork. Finally, the higher roughness of the masonry with deep joints (S12R-BMJ-200 series) led to the highest value of η (28.8%). In every instance, due to the weaker mechanical properties of the substrates, the exploitation ratios are lower than those derived on concrete with the same reinforcement system (S12R).

The load-slip response curves are plotted in Fig. 12. Figs. 12a and 12c show the comparison between the slip measurements obtained from LVDTs and DIC. In the former (Fig. 12a) the curves refer to one specimen of S12R-CB-200 series (steel textile with 12 cord/in bonded to clay brick) and one of S12R-TU-200 (tuff substrate) are represented, while in the latter (Fig. 12c) a specimen of S12R-BMJ-200 (on masonry prism with deep joints) is shown. A good agreement was found between the two measurements, with a slight mismatch only at very low slip values, due to the noise of DIC data. Both in the plots in Figs. 12b (all tests on tuff and clay brick substrates) and 12d (all tests on masonry prisms) and in Table 5, the slip is measured by LVDT transducers.

Apart from the differences in terms of maximum load, already discussed beforehand, the load-slip curves indicate that:

(i) the response on irregular surfaces (masonry substrates, Fig. 12d) is more brittle than that on homogeneous substrates (tuff and clay brick, Fig. 12b), as revealed by both the shape of the curve and the ultimate slip, at which the complete detachment occurred and test finished (about 0.4mm on tuff and brick and 0.2-0.25mm on masonry);

(ii) despite the large difference in terms of maximum force, the slip at peak load recorded on tuff substrate is comparable to that measured on clay brick, due to the larger deformability of the tuff with respect to the brick;

(iii) the curves recorded on masonry are characterized by load drops corresponding to the debonding process progressively crossing the mortar joints, especially on the longer bonded length (L_b=280mm), even if this trend is not clearly detectable in all tests;
(iv) the slip values at peak load measured on masonry (0.18-0.24mm, Table 5) are lower than those recorded on concrete (2-3.6mm, Table 4), due to the lower maximum load per unit width F_b* (7.8-9kN/m versus 26.8-30.8kN/m);
(v) the slip at peak load recorded on both clay brick and brick masonry (0.18-0.24mm) are lower than those measured in previous studies (about 0.25-0.35mm, [12]), in which tests were carried out using the same textile and the same substrates, but a more deformable epoxy resin (E_m=1.3-1.6kN/mm^2 versus E_m=3.2kN/mm^2).

The strain profiles along the centre line of the SRP reinforcements and the strain fields on the surface of the specimens, both recorded by the Digital Image Correlation, are depicted in Figs. 13 and 14 (for the same specimens), providing information on the effective bond length and on the distribution of the stresses and their evolution during load application:

(i) on brick substrate, the strain profiles recorded at 90% and 100% F_b exhibit a change in the concavity with respect to the profiles recorded at lower loads, indicating that the debonding process has activated. The curves approximately reach the zero at about 160-180mm, which provides an estimate of the effective bond length (Figs. 13a and 14a), in agreement with that (160-200mm) suggested by previous studies [12];
(ii) the strain profile (Fig. 14b) and the strain field (Fig. 14b) on brickwork clearly show that the inhomogeneity of the substrate induces a strongly uneven strain distribution, with a periodic variation related to the alternation of brick units and mortar joints [41,42]. Stress transfer is concentrated at the brick surface, while it strongly reduces at the bed joints, due to the lower stiffness of the mortar with respect to the brick. This also indicates that the SRP-to-masonry substrate load transfer mechanism mainly relies on the brick rather than on the mortar. Therefore, the design relationship for the estimate of the bond strength should account for the mechanical properties of the brick, rather than for the average (global) properties of the brickwork assembly;
(iii) due to the variability of the strain profile, it is more difficult to provide an estimate of the effective bond length on brickwork. From the curves in Fig. 13b, it can be roughly estimated to be about 150-160mm, confirming the former observations made on the base of the maximum loads achieved with L_b=200mm and L_b=280mm;
(iv) the brick substrate is progressively engaged during load application (Fig. 14a), while the bricks of the masonry prisms are suddenly involved in the load transfer as soon as the stress crosses a mortar joint (see the strain profiles in Fig. 14b at 60% and 80% and again at 80% and 100% F_b);
(v) the strain at the loaded end at 100% F_b (0.41% on brick, Fig. 12a, and 0.57% on masonry, Fig. 13b) approximately matches the elastic strain of the steel textile under the applied load (7.6kN and 11.6kN). However, higher strains concentrated at about 50mm from the loaded end (at the second brick) of the masonry prisms.
(vi) The strain measured by DIC at debonding on the midline of the bonded area was higher that the theoretical maximum value $F_b/(A_fE_t)$, which is a mean strain widthwise, suggesting that the SRP-to-substrate stress transfer zone concentrates in the middle of the bonded area with lower stresses being transferred at the edges. This mismatch was higher on brick/masonry substrates than on concrete, probably because of the smaller width of the bonded area (50mm instead of 100mm).

5. COMPARISON WITH STANDARD CODES AND CALIBRATION OF DESIGN COEFFICIENTS

The Italian Guidelines CNR DT-200 [24] provide a design relationship to estimate the bond strength of externally bonded FRP reinforcements, explicitly referring to end debonding, differently from the US ACI guides [22,23] in which intermediate debonding is assumed to occur in shear-controlled failure modes. According to [24], the theoretical debonding load ($F_{b,th}$) is estimated on the base of the mechanical properties of both the substrate (compressive strength f_{cs} and tensile strength f_{ts}) and the FRP (tensile modulus of elasticity E_t and design thickness t), as follows:

$$F_{b,th} = b_f \sqrt{2E_t t k_b k_G \sqrt{f_{cs} f_{ts}}} \quad (1)$$

in which b_f is the width of the reinforcement strip, k_b is the scalar coefficient accounting for width effects (as said beforehand), and k_G is a tuning coefficient (with the dimensions of a length) calibrated on experimental basis by using the data available in the scientific literature. Both average and characteristic values (5% fractile) of k_G are provided separately for concrete, brick and tuff substrates.

In this section, k_G is calibrated according to the "Design by testing" approach recommended by the Annex D of Eurocode 0 [43], in order to investigate if the coefficients provided for carbon, glass and aramid FRP reinforcements can be extended to SRPs, or, otherwise, need to be purposely recalibrated. To this aim, the experimental data published in the literature on the SRP-to-substrate bond strength are collected together with those derived in the present study, for concrete (Table 6) and brick/brickwork (Table 7) substrates; in these Tables, N is the number of tests, b is width of the substrate, f_{cs} and f_{ts} are mean cylindrical compressive strength and mean tensile strength of the substrate, respectively, L_b and b_f are the bonded length and the bonded width, respectively, E_t is the Young's modulus of SRP, and, finally, $F_{b,exp}$ and $\sigma_{b,exp}$ are the experimental debonding load and the corresponding stress in the textile. Tests collected in the databases were performed on SRP reinforcements comprising different epoxy resins and steel textiles. These latter ones were made out of brass- or zinc- coated cords of UHTSS steel, having density ranging from 4 to 23 cord/in. In general, the databases include both single-lap and double-lap tests, since it was found that they lead to similar results, provided that proper alignment and uniform load distribution between the two sides of the specimen are ensured in double-lap tests [11].The recalibration of k_G was not attempted for tuff substrates, due to the lack of available experimental data. The tests are grouped in datasets, each gathering N tests with nominally identical testing setup, geometry and mechanical properties of the substrate, and configuration and mechanical properties of the SRP reinforcement.

The experimental values of the debonding load ($F_{b,exp}$) are interpolated with a least-square regression line through the origin to fit theoretical values $F_{b,th}$ evaluated for k_G=1. Then, the mean value k_{Gm} (which is under square root in the expression of F_{th} in Eq. 1) is obtained as the slope of the regression line to the power of 2:

$$k_{Gm} = \left(\frac{\sum_i F_{b,exp}^i F_{b,th}^i}{\sum_i \left(F_{b,th}^i\right)^2} \right)^2 \tag{2}$$

The characteristic (5% percentile) coefficient k_{Gk} is evaluated assuming that the error function (ratio between experimental and theoretical values) has a log-normal distribution with mean μ_Δ and variance s_Δ:

$$\sqrt{k_{Gk}} = \sqrt{k_{Gm}} \cdot \exp\left(\mu_\Delta - k_n s_\Delta - 0.5 {s_\Delta}^2\right) \tag{3}$$

where the characteristic fractile factor of the Gaussian distribution (k_n) depends on the number of specimens [43]. Table 6 collects the works presenting experimental investigations on the bond strength of SRP on concrete, performed with a bonded length at least equal to the effective one. Totally, including the results of this study, 34 tests are considered, grouped into 16 datasets. In the design relationship, the mechanical properties of the substrates are the mean cylindrical compressive strength (f_{cs}) and the tensile strength (f_{ts}). Therefore, for those papers that do not provide them directly (e.g., the cubic compressive strength is reported, or no tensile strength is indicated) the expressions recommended by the Italian building code [32] are used.

The resulting mean value of the tuning coefficient is k_{Gm}=0.087mm, while the characteristic one is k_{Gk}=0.038mm (the fractile factor is k_n=1.7). The comparison between experimental results and corresponding theoretical estimate is shown in Fig. 15a, together with the mean and characteristic regression lines. The mean coefficient is slightly higher than that provided by the Italian guidelines (0.077mm), while the characteristic one practically coincides (0.037mm). The ratio k_{Gk}/k_{Gm}=0.038/0.087=0.44 is slightly lower than that of the guidelines (0.48), because the theoretical relationship underestimates the bond strength of SRP comprising low density textiles (with 4 cord/in), causing a relatively larger dispersion of data.

The results of the bond tests carried out on brick/brickwork substrate are collected in Table 7, for a total of 108 tests, grouped in 30 datasets, whereas the comparison between experimental results and corresponding theoretical estimate is shown in Fig. 15b. The normalized values of the compressive strength of the substrate (f_{cs}) was used, according to the Annex A of the European Standard EN 772-1 [44], applying the geometric conversion coefficient to the strength values reported in the cited papers, if necessary. The tensile strength (f_{ts}), if not specified (i.e., if it was not provided by the papers on the base of experimental results), was derived from f_{cs} according to the relationship recommended by the Italian Building Code [33] for concrete, and assumed equal to $0.1f_{cs}$ for clay bricks. Most of the results were derived within two Round Robin Test

programs organized by the Rilem TC 223-MSC (Masonry Strengthening with Composites [11]) and the Rilem TC 250-CSM (Composites for the Sustainable strengthening of Masonry [12]). For the tests carried out within these two Round Robin programs and this study, the orthogonal and the parallel compressive strength values are considered for tests on brick and on masonry substrates, respectively. According to the observations made in the previous section, the properties of the brick only are considered, rather than those of the masonry assembly. The tests carried out on clay bricks with L_b=160mm [11] are included even though such bonded length is slightly lower than the effective one [12]. The mean value of the tuning coefficient results k_{Gm}=0.052mm, which is lower than that provided by the Italian Guidelines (0.093mm, [24]), but agrees with that (0.050mm) suggested by recent works [45-47] on the base of a wider database. The characteristic coefficient is k_{Gk}=0.017mm (k_n=1.645, k_{Gk}/k_{Gm}=0.33) that, again, is lower than that of the guidelines (0.031mm, [24]) and matches those recently proposed for FRPs (0.015mm [46], 0.017mm [47]). The dispersions of data for all these calibrations also coincide, k_{Gk}/k_{Gm} being comprised between 0.30 and 0.34. Clearly, a larger number of experimental results on the bond strength of SRPs may lead to a more precise calibration of the design coefficients and to improved comparisons with carbon and glass FRPs, for which a more consolidated knowledge has already been developed. Furthermore, experimental data on other substrates with relevant perspective applications of SRP in the field, such as tuff, limestone, and timber, are still lacking.

6. CONCLUSIONS

An experimental investigation was carried out on the tensile and bond behaviour of three SRP systems comprising UHTSS textiles with 4, 12 and 18 cord/in densities and a bi-component epoxy resin. The steel textiles have a tensile strength of 3100-3200N/mm^2 and a Young's modulus is 182kN/mm^2. The strength of SRP composites matches that of dry textiles, while the resin leads to slightly higher values of the Young's modulus (225-230kN/mm^2) and to lower peak strains (1.90-1.95% versus 2.1-2.2%).
Single-lap bond tests were carried out on high and low strength concrete, tuff, clay brick, and brickwork substrates, providing information on the main issues related to the design of externally bonded SRP reinforcements.

(i) Shear bond strength and failure mode

- The debonding loads (per unit width) achieved on concrete substrates varied between 206kN/m and 326kN/m and grew with the increase of the density of the textile and of the strength of the substrate.
- The bond strength was 55kN/m on tuff and 132kN/m on clay brick. On masonry, the mortar joints produced an interlocking effect leading to a strength increase of 14%, and of nearly 50% (195kN/m) with improved roughness.
- The failure mode consists in cohesive debonding with detachment of a thin and uniform layer of substrate on concrete, tuff and brick, while the surface of masonry involved in the detachment is slightly irregular, due to the unit/joint variation.

(ii) Effective transfer length

The effective transfer length of SRP was estimated to be 130-150mm for S4R and 150-170mm for S12R and S18R on concrete, 160-180mm on brick and 150-160mm on masonry. The SRP-to-masonry load transfer mechanism mainly relies on the brick rather than on the mortar. Therefore, the design relationship for the estimate of the bond strength should account for the mechanical properties of the brick, rather than for the average properties of the brickwork assembly.

(iii) Calibration of design coefficients

The average and characteristic tuning coefficients (k_{Gm} and k_{Gk}) for the determination of the bond strength according to the relationship of the Italian Guidelines on FRPs [24] were calibrated on the base of the experimental results derived in this study and those available in the scientific literature.

- As for concrete substrates, k_{Gm}=0.087mm and k_{Gk}=0.038mm.
- As for brick/masonry substrates, k_{Gm}=0.052mm and k_{Gk}=0.017mm.
- These coefficients basically agree with those suggested for carbon and glass FRPs by [24] for concrete and by the most recent studies [24,45-47] for brick/masonry.

The behaviour of SRP systems appears analogous to that of Carbon, Glass and Aramid FRPs, which are included in the existing guidelines for qualification and design. Further investigations may allow for a more precise calibration of the design coefficients and for the collection of data on the bond strength of SRP on other substrates with relevant perspective applications in the field, such as tuff, limestone, and timber.

ACKNOWLEDGEMENTS

This work was carried out under the research project ReLUIS-DPC 2015, Thematic Area Innovative materials for interventions in seismic areas. Kerakoll S.p.A. provided materials and funding. The technical cooperation of Dr. Paolo Casadei is gratefully acknowledged.

REFERENCES

[1] Barton B, Wobbe B, Dharani LR, Silva P, Birman V, Nanni A, Alkhrdaji T, Thomas J, Tunis G. Characterization of RC Beams Strengthened by Steel Reinforced Polymer and Grout (SRP & SRG) Composites. In: Proceedings of Int. Conference on Recent Advances in Composite Materials, Varanasi, India, 2004.

[2] Borri A, Castori G. Indagini sperimentali sulla durabilità di materiali compositi in fibra d'acciaio. In: Proceedings of XIV Convegno ANIDIS, Bari, 2011 (in Italian).

[3] De Santis S, de Felice G. Steel reinforced grout systems for the strengthening of masonry structures. Composite Structures 2015;134:533-548. DOI: 10.1016/j.compstruct.2015.08.094.

[4] Figeys W, Schueremans L, Brosens K, Van Gemert D., 2005. Strengthening of concrete structures using steel wire reinforcement polymer. ACI Special Publication 2005;230:743-762.

[5] Matana M, Nanni A, Dharani LR, Silva P, Tunis G. Bond Performance of steel reinforced polymer and steel reinforced grout. In: Proceedings Int. Symposium on Bond Behaviour of FRP in Structures (BBFS), Hong Kong, China, 2005.

[6] Manos GC, Katakalos K, Kourtides V. The influence of concrete surface preparation when fiber reinforced polymers with different anchoring devices are being applied for strengthening R/C structural members. Applied Mechanics and Materials 2011;82:600-605. DOI: 10.4028/www.scientific.net/AMM.82.600.

[7] Stievanin E, da Porto F, Panizza M, Garbin E, Modena C. Bond characterization between historical concrete substrate and SRG/SRP strengthening systems. In: Proceedings of 5th Int. Conference on Structural Engineering, Mechanics and Computation SEMC2013, Cape Town, South Africa, 2013.

[8] Cancelli AN, Aiello MA, Casadei P. Experimental investigation on bond properties of SRP/SRG-masonry systems. In: Proceedings of FRPRCS-8, Patras, Greece, 2007.

[9] Capozucca R. Experimental FRP/SRP-historic masonry delamination. Composite Structures 2010;92(4):891-903. DOI: 10.1016/j.compstruct.2009.09.029.

[10] Grande E, Imbimbo M, Sacco E. Bond behavior of historical clay bricks strengthened with steel reinforced polymers (SRP). Materials 2011;4(3):585-600. http://dx.doi.org

[11] Valluzzi MR, Oliveira DV, Caratelli A, Castori G, Corradi M, de Felice G, Garbin E, Garcia D, Garmendia L, Grande E, Ianniruberto, U, Kwiecień A, Leone M, Lignola GP, Lourenço PB, Malena M, Micelli, F, Panizza, M, Papanicolaou CG, Prota A, Sacco E, Triantafillou TC, Viskovic A, Zając B, Zuccarino G. Round robin test for composite to brick shear bond characterization. Materials and Structures 2012;45:1761-1791. DOI: 10.1617/s11527-012-9883-5.

[12] de Felice G, Aiello MA, Bellini A, Ceroni F, De Santis S, Garbin E, Leone M, Lignola GP, Malena M, Mazzotti C, Panizza M, Valluzzi MR. Composite-to-brick masonry shear bond. Materials and Structures 2015. DOI: 10.1617/s11527-015-0669-4.

[13] Mitolidis GJ, Salonikios TN, Kappos AJ. Test results and strength estimation of R/C beams strengthened against flexural or shear failure by the use of SRP and CFRP. Composites Part B: Engineering 2012;43(3):1117-1129. DOI: 10.1016/j.compositesb.2011.11.034.

[14] Abdelrahman, K, El-Hacha R. Behavior of large-scale concrete columns wrapped with CFRP and

SFRP sheets. J Compos Constr 2012;16(4):430-439. DOI: 10.1061/(ASCE)CC.1943-5614.0000278.
[15] Napoli A, Realfonzo R. Reinforced concrete beams strengthened with SRP/SRG systems: Experimental investigation. Construction and Building Materials 2015;93:654-677. DOI: 10.1016/j.conbuildmat.2015.06.027.
[16] Napoli A, Realfonzo, R. Compressive Behaviour of Concrete Confined by SRP Wraps. Construction and Building Materials. DOI: 10.1016/j.conbuildmat.2016.01.055.
[17] Balsamo A, Nardone F, Iovinella I, Ceroni F, Pecce M. Flexural strengthening of concrete beams with EB- FRP, SRP and SRCM: experimental investigation. Composites Part B: Engineering 2013:46:91-101. DOI: 10.1016/j.compositesb.2012.10.014.
[18] Borri A, Casadei P, Castori G. Hammond J. Strengthening of brick masonry arches with externally bonded steel reinforced composites. Journal of Composites for Construction 2009;13(6):468-475. DOI: 10.1061/(ASCE)CC.1943-5614.0000030.
[19] Borri A, Castori G, Corradi M. Masonry columns confined by steel fiber composite wraps. Materials 2011;4:311-326. DOI: 10.3390/ma4010311.
[20] Valluzzi MR, da Porto F, Garbin E, Panizza M. Out-of-plane behaviour of infill masonry panels strengthened with composite materials. Materials and Structures 2014;47(12):2131-2145. DOI: 10.1617/s11527-014-0384-6.
[21] FIB, Fédération internationale du béton. Fib Bulletin No. 14. Externally bonded FRP reinforcement for RC structures. Lausanne, Switzerland, 2001.
[22] American Concrete Institute. ACI 440.2R-08 Guide for the design and construction of externally bonded FRP systems for strengthening concrete structures. Farmington Hills, MI, USA, 2008.
[23] American Concrete Institute. ACI 440.7R-10 Guide for the design and construction of externally bonded Fibre-Reinforced polymer systems for strengthening unreinforced masonry structures. Farmington Hills, MI, USA, 2010.
[24] CNR Italian National Research Council. CNR-DT200 R1/2013. Guide for the design and construction of externally bonded FRP systems for strengthening existing structures. Rome, 2013.
[25] de Felice G, De Santis S, Napoli A, Realfonzo R. Overview of the experimental works on steel reinforced polymer systems. In: Proceedings of ACE 2015 2nd International Symposium on Advances in Civil Engineering. 12-13 June 2015, Vietri sul Mare, Italy.
[26] Bencardino F, Condello A. SRG/SRP-concrete bond-slip laws for externally strengthened RC beams. Composite Structures 2015;132:804-815. DOI: 10.1016/j.compstruct.2015.06.068.
[27] Hardwire LLC - web site: <www.hardwirellc.com> [accessed Nov 2015].
[28] Kerakoll S.p.A. - web site: <www.kerakoll.com> [accessed Nov 2015].
[29] De Santis S, de Felice G. Tensile behaviour of mortar-based composites for externally bonded reinforcement systems. Composites Part B: Engineering 2015;68:401-413. DOI: 10.1016/j.compositesb.2014.09.011.
[30] Pan B, Qian K, Xie H, Asundi A. Two-dimensional digital image correlation for in-plane displacement and strain measurement: a review. Measurement Science and Technology 2009;20(6)062001. DOI: 10.1088/0957-0233/20/6/062001.
[31] UNI EN 2561:1995. Aerospace series - Carbon fibre reinforced plastics - Unidirectional laminates - Tensile test parallel to the fibre direction.
[32] de Felice G, De Santis S, Garmendia L, Ghiassi B, Larrinaga P, Lourenço PB, Oliveira DV, Paolacci F, Papanicolaou CG. Mortar-based systems for externally bonded strengthening of masonry. Materials and Structures 2014;47:2021-2037. DOI 10.1617/s11527-014-0360-1.
[33] Ministry of Infrastructure and Transport. Nuove norme tecniche per le costruzioni (DM 14/01/2008). Gazzetta Ufficiale della Repubblica Italiana n.47, Supplemento Ordinario n.27. Consiglio Superiore dei Lavori Pubblici: Rome, Italy, 2009 (Italian Standard, in Italian).
[34] UNI EN 772-1:2011. Methods of test for masonry units. Determination of compressive strength.
[35] Yao J, Teng JG, Chen JF. Experimental study on FRP-to-concrete bonded joints. Composites Part B: Engineering 2005; 36(2):99-113. DOI: 10.1016/j.compositesb.2004.06.001.
[36] Pellegrino C, Tinazzi D, Modena C. Experimental study on bond behavior between concrete and FRP reinforcement. Journal of Composites for Construction 2008;12(2):180-189. DOI: 10.1061/(ASCE)1090-0268(2008)12:2(180).
[37] Mazzotti C, Savoia M, Ferracuti B. An experimental study on delamination of FRP plates bonded to concrete. Construction and Building Materials 2008;22(7):1409-1421. DOI: 10.1016/j.conbuildmat.2007.04.009.
[38] Kurihashi Y, Mikami H, Komuro M, Kishi N. Strengthening effects of bonding AFRP plate on

flexural capacity of RC beams for submerged application. Proceedings of the 13th East Asia-Pacific Conference on Structural Engineering and Construction, EASEC 2013.

[39] Aiello MA, Sciolti SM. Bond analysis of masonry structures strengthened with CFRP sheets. Construction and Building Materials 2006;20(1-2):90-100. DOI: 10.1016/j.conbuildmat.2005.06.040.

[40] Oliveira D, Basilio I, Lourenço P. Experimental Bond Behavior of FRP Sheets Glued on Brick Masonry. Journal of Composites for Construction 2011;15(1):32-41. DOI: 10.1061/(ASCE)CC.1943-5614.0000147.

[41] Focacci F, Carloni C. Periodic variation of the transferable load at the FRP-masonry interface. Composite Structures 2015;129:90-100. DOI: 10.1016/j.compstruct.2015.03.008.

[42] Mazzotti C, Murgo FS. Numerical and experimental study of GFRP-masonry interface behavior: bond evolution and role of the mortar layers. Composites Part B: Engineering 2015;75:212-225. DOI: 10.1016/j.compositesb.2015.01.034.

[43] CEN, European Committee for Standardization. EN 1990:2002. Eurocode 0: Basis of structural design.

[44] CEN, European Committee for Standardization. EN 772-1:2011. Methods of test for masonry units. Determination of compressive strength.

[45] Ceroni F, Ferracuti B, Savoia M, Pecce M. Assessment of a bond strength model for FRP reinforcement externally bonded over masonry blocks. Composites Part B: Engineering 2014;61:147-161. DOI: 10.1016/j.compositesb.2014.01.028.

[46] Ceroni F, Ferracuti B, Pecce M, Savoia M. Corrigendum to ‘‘Assessment of a bond strength model for FRP reinforcement externally bonded over masonry blocks’’ [Composites Part B: Engineering 2014; 61: 147–161]. Composites Part B: Engineering 2015;69:612. DOI: 10.1016/j.compositesb.2014.08.053.

[47] Sacco, E. Personal communication.

Figure captions

Figure 1. Ultra High Tensile Strength Steel (UHTSS) textiles: detail of the steel cord (a), textiles with 4 cord/in (S4, b), 12 cord/in (S12, c) and 18 cord/in (S18, d).

Figure 2. Testing setup for tensile tests on dry textile (a) and SRP composite (b) specimens.

Figure 3. Stress-strain response curves of tensile tests: comparisons between different displacement/strain measurement methods (a, e, f) and results of tests on dry textile and SRP composites (b,d,f): S4 and S4R (a,b), S12 and S12R (c,d), and S18 and S18R (e,f).

Figure 4. Prisms of brick masonry made of four (a) or five (b) half brick layers for shear tests with bonded length Lb=200mm and Lb=280mm, respectively.

Figure 5. Testing setup for shear bond tests on concrete (a) and masonry (b) substrates.

Figure 6. Comparisons between direct slip measurement with laser transducers and indirect slip measurement from the LVDT integrated in the testing machine for one specimen of S12R-HSC-300 (a) and S18R-HSC-150 (b) series.

Figure 7. Load-slip curves of shear bond tests on SRP reinforcements on concrete substrates: S12R-HSC (a), S12R-LSC (b) and S18R-HSC (c) series.

Figure 8. Load-slip curves of shear bond tests on systems applied on concrete substrates: influence of the textile density for L_b=150mm (a) and L_b=300mm (b).

Figure 9. Failure mode exhibited by SRP on concrete (a), tuff (b), brick (c) and brickwork (d) substrates in shear bond tests.

Figure 10. Strain profiles (from resistive strain gauge measurements) along the bonded area of SRP reinforcements with S4 textile bonded to low strength concrete substrate.

Figure 11. Strain profiles (from resistive strain gauge measurements) along the bonded area of SRP reinforcements with S12 (a,c,e) and S18 (b,d,f) textiles, bonded to high (a,b) and low (c,d,e,f) strength concrete substrates.

Figure 12. Load-slip curves of shear bond tests on systems applied on brick/brickwork (a,b) and tuff (c,d) substrates: comparison between LVDT and DIC measurements (a,c) and load-slip curves of all experimental tests (b,d).

Figure 13. Strain profiles (from Digital Image Correlation) along the bonded area of SRP reinforcements bonded to brick (a) and brickwork (b) substrates.

Figure 14. Strain field (from Digital Image Correlation) of the SRP strip and of the substrate in shear bond tests on brick (a) and brickwork (b) substrates

Figure 15. Experimental vs. theoretical bond strength on concrete (a) and brick/brickwork (b) substrates.

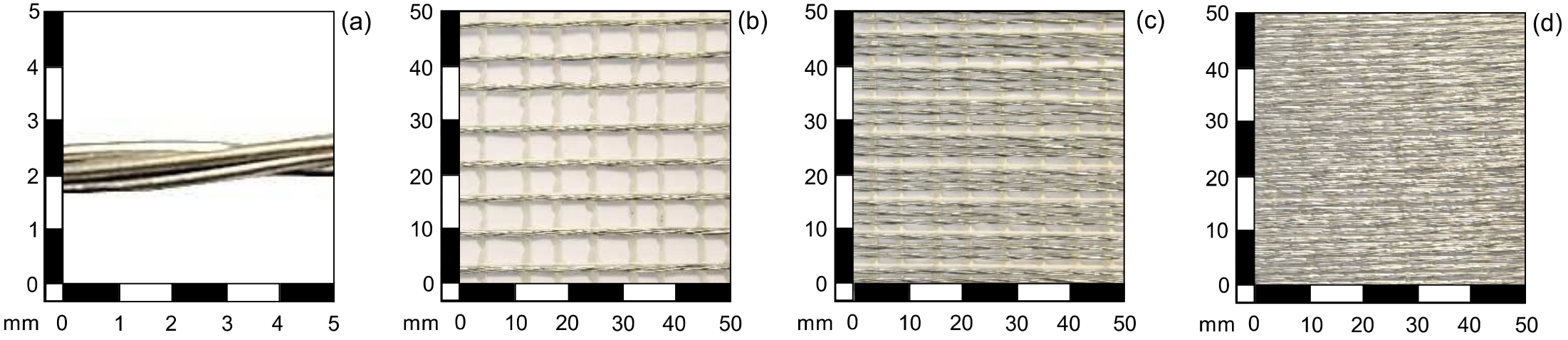
(a)
5
4
3
2
1
0
mm 0 1 2 3 4 5
(b)
50
40
30
20
10
0
mm 0 10 20 30 40 50
(c)
50
40
30
20
10
0
mm 0 10 20 30 40 50
(d)
50
40
30
20
10
0
mm 0 10 20 30 40 50

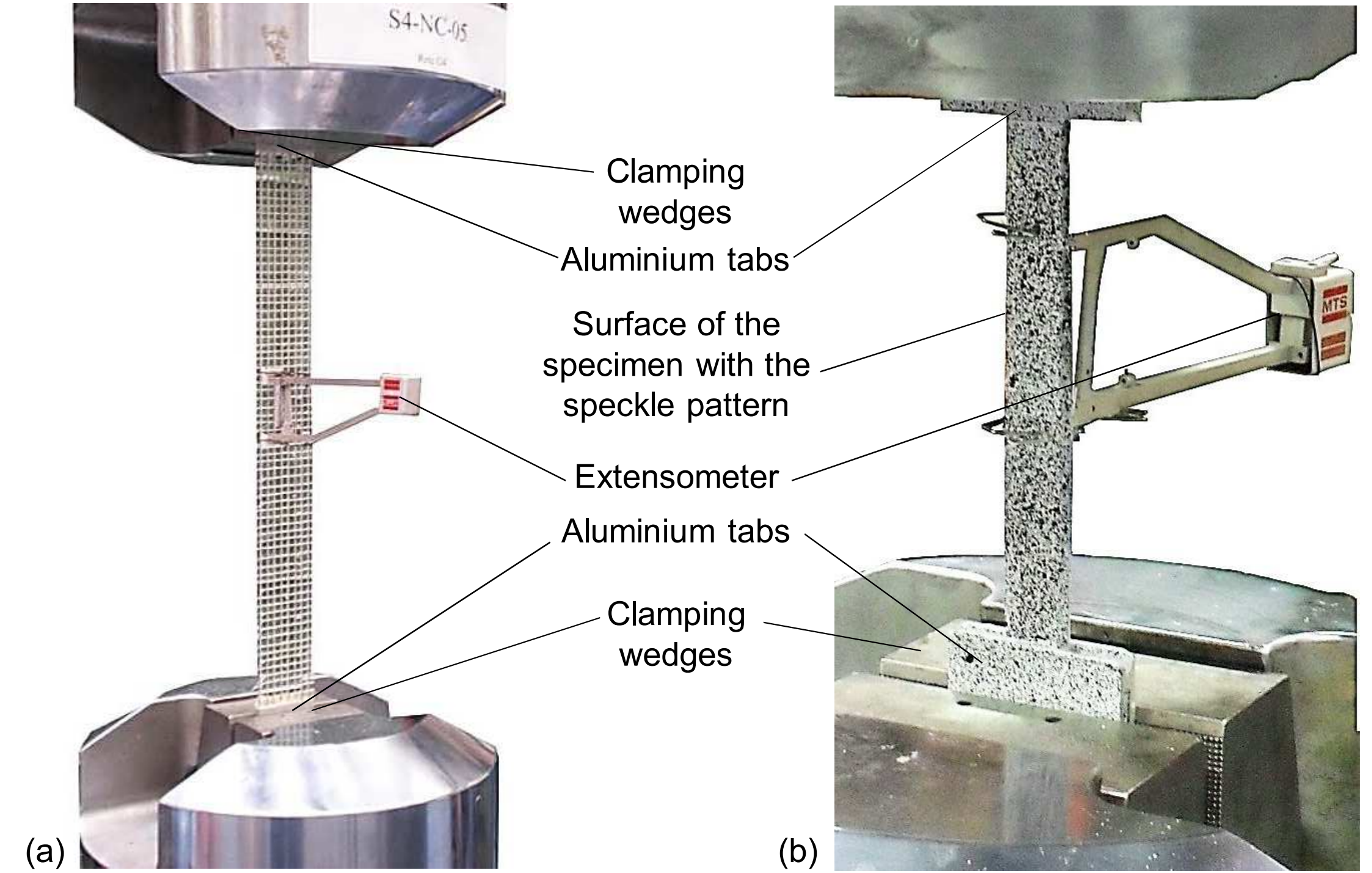
S4-NC-05
Clamping wedges
Aluminium tabs
Surface of the specimen with the speckle pattern
Extensometer
Aluminium tabs
Clamping wedges
MTS
(a)
(b)

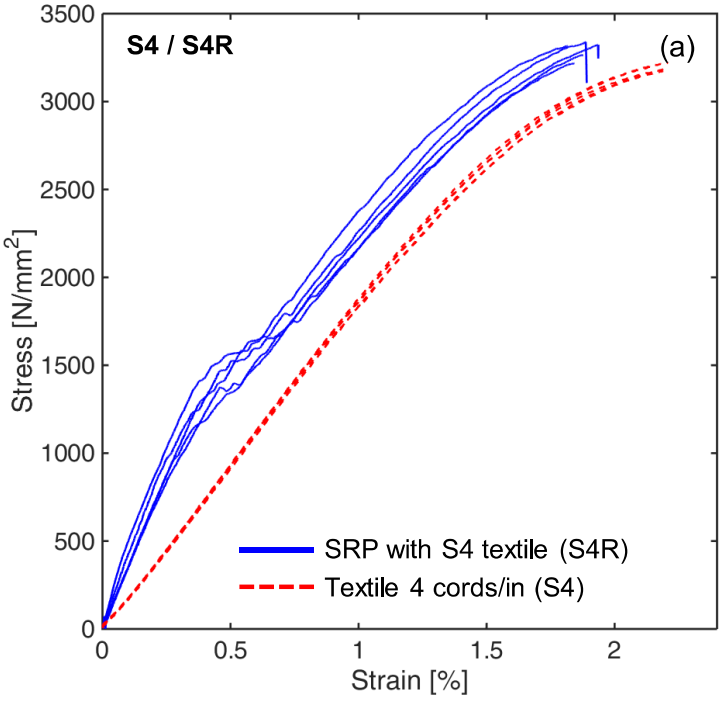
S4 / S4R
(a)
Stress [N/mm^2]
Strain [%]
SRP with S4 textile (S4R)
Textile 4 cords/in (S4)

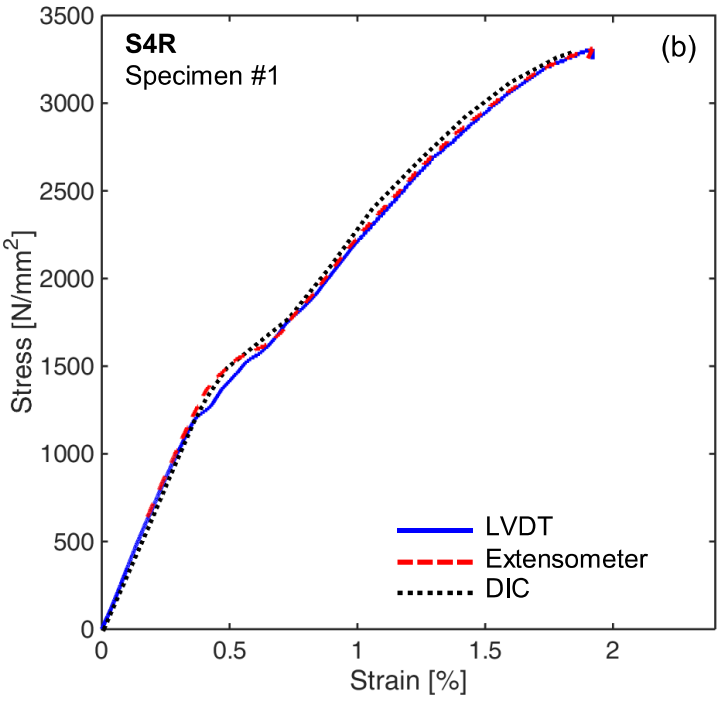
S4R
Specimen #1
(b)
Stress [N/mm^2]
Strain [%]
LVDT
Extensometer
DIC

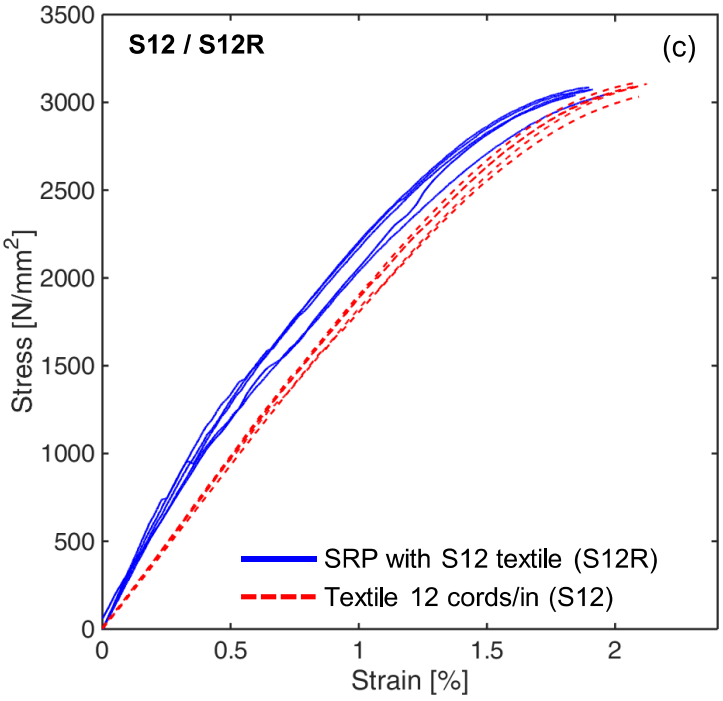
S12 / S12R
(c)
Stress [N/mm^2]
Strain [%]
SRP with S12 textile (S12R)
Textile 12 cords/in (S12)

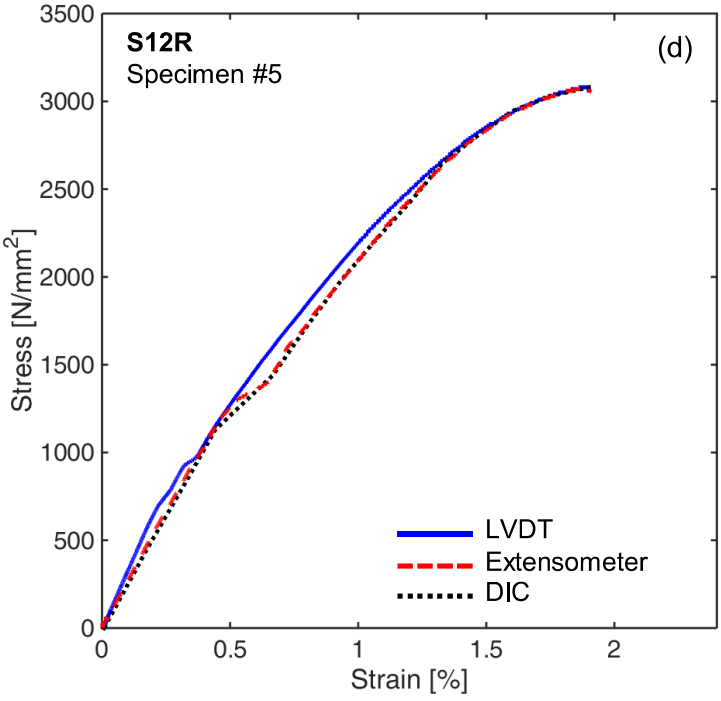
S12R
Specimen #5
(d)
Stress [N/mm^2]
Strain [%]
LVDT
Extensometer
DIC

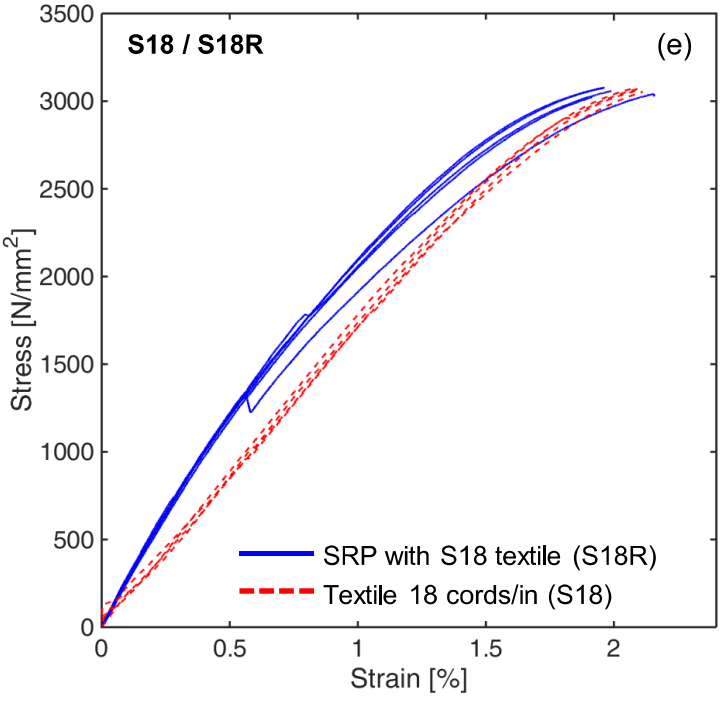
S18 / S18R
(e)
Stress [N/mm^2]
Strain [%]
SRP with S18 textile (S18R)
Textile 18 cords/in (S18)

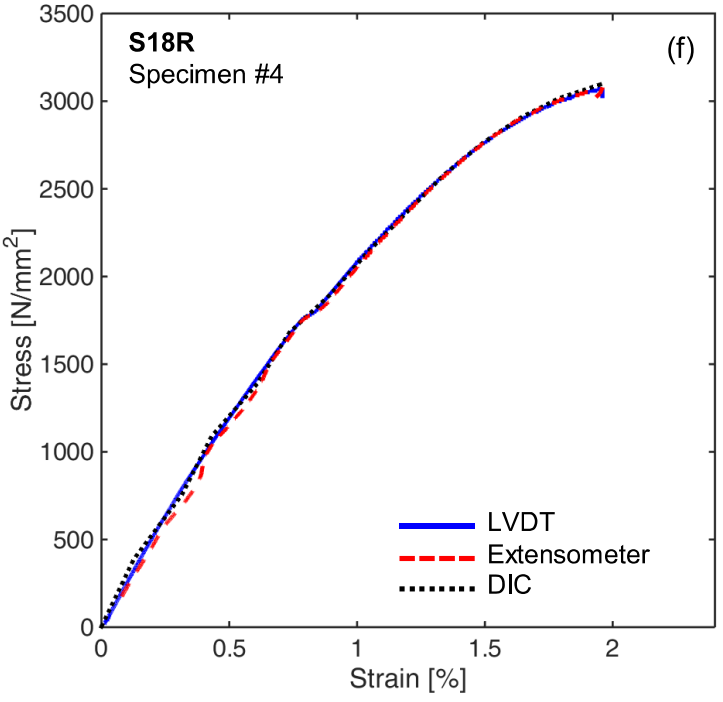
S18R
Specimen #4
(f)
Stress [N/mm^2]
Strain [%]
LVDT
Extensometer
DIC

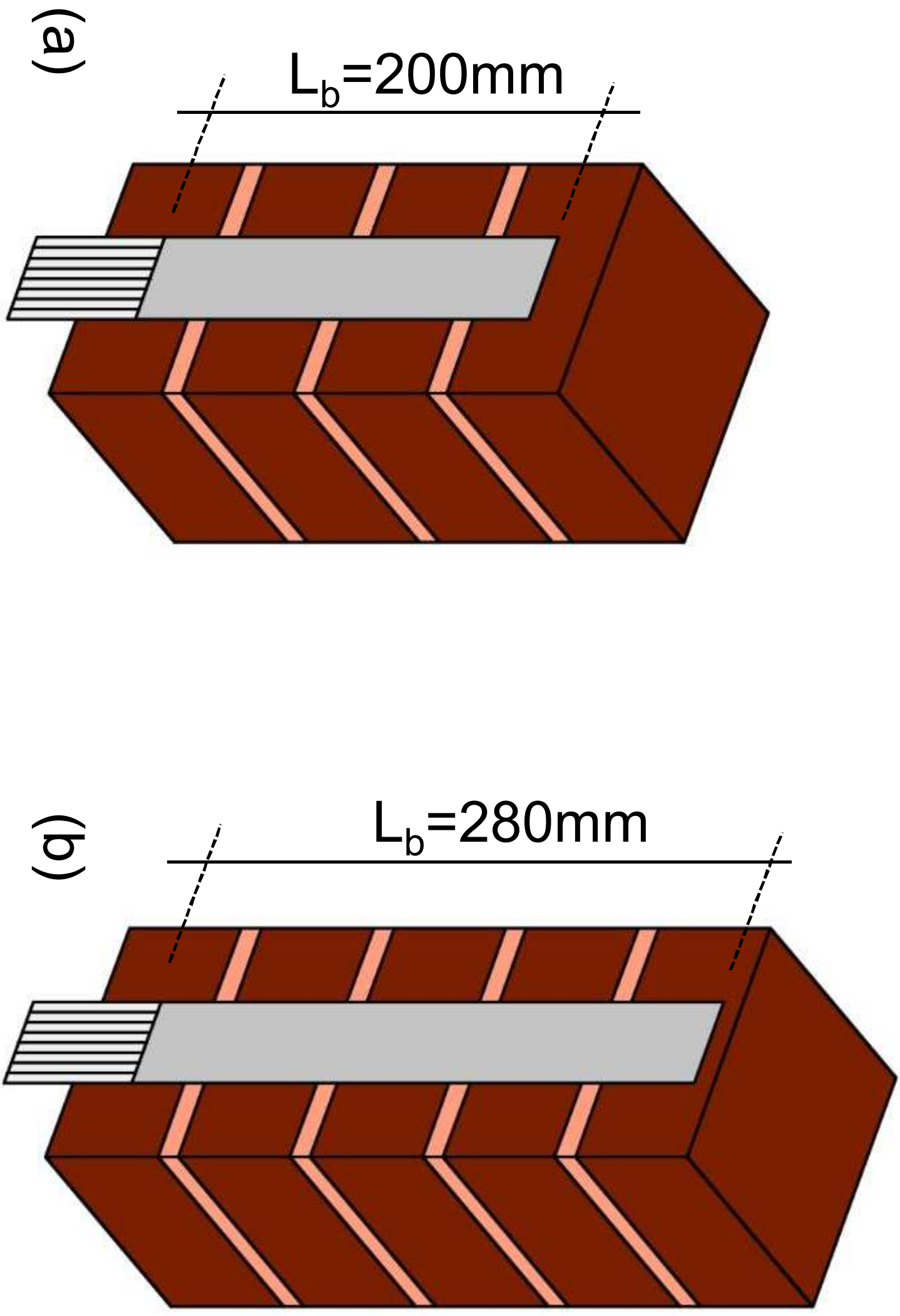
(a)
L_b=200mm
(d)
L_b=280mm

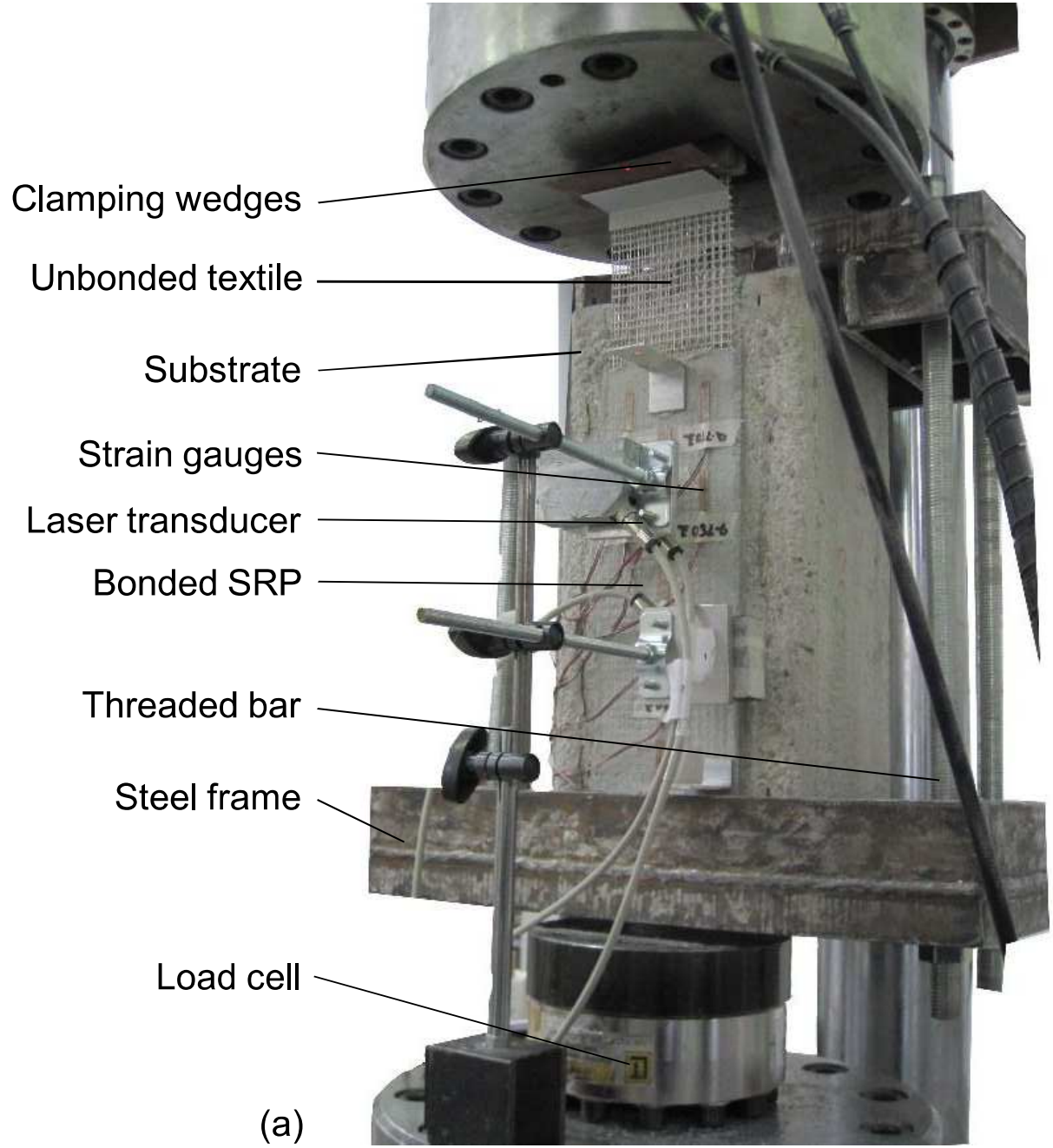
Clamping wedges
Unbonded textile
Substrate
Strain gauges
Laser transducer
Bonded SRP
Threaded bar
Steel frame
Load cell
(a)

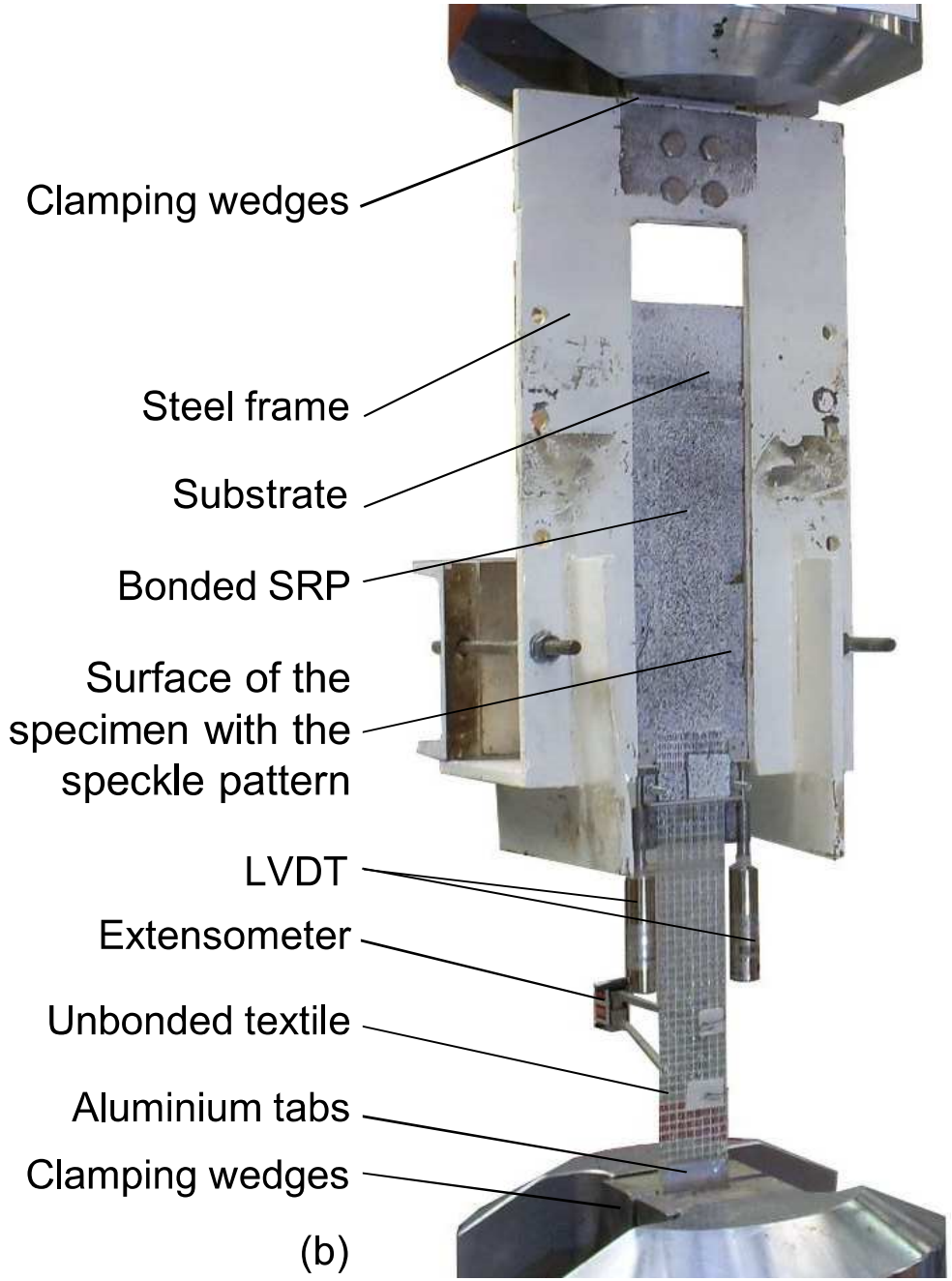
Clamping wedges
Steel frame
Substrate
Bonded SRP
Surface of the specimen with the speckle pattern
LVDT
Extensometer
Unbonded textile
Aluminium tabs
Clamping wedges
(b)

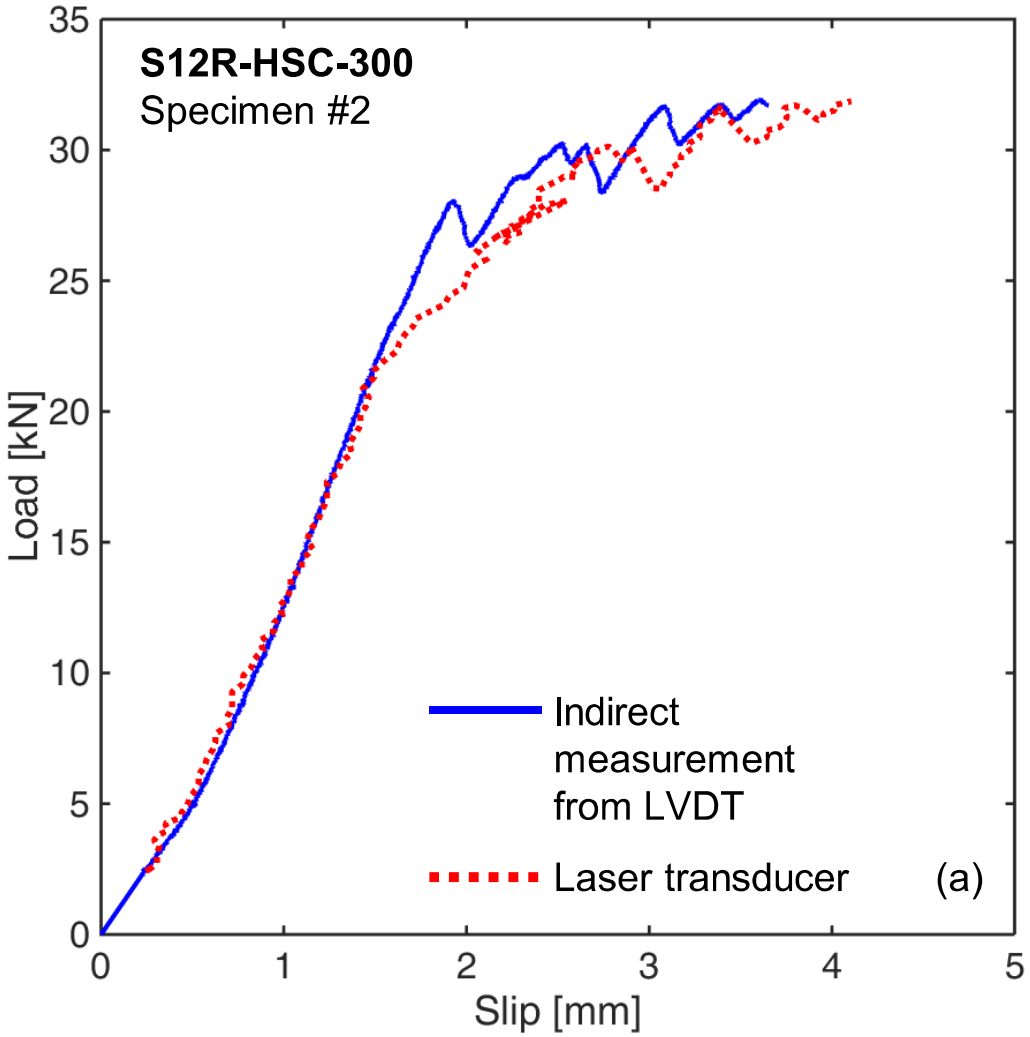
S12R-HSC-300
Specimen #2
Load [kN]
Slip [mm]
Indirect measurement from LVDT
Laser transducer
(a)
0
5
10
15
20
25
30
35
0
1
2
3
4
5

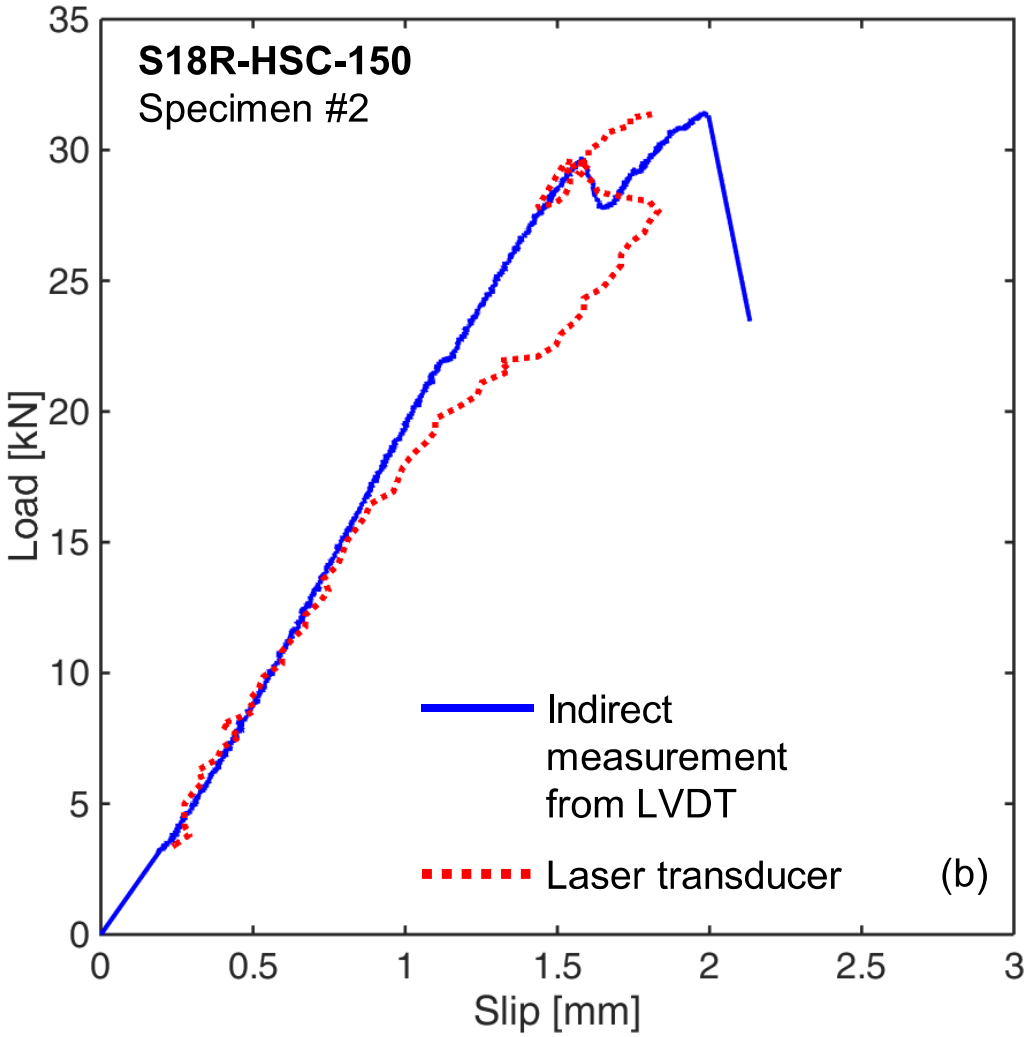
S18R-HSC-150
Specimen #2
Load [kN]
Slip [mm]
Indirect measurement from LVDT
Laser transducer
(b)
0
5
10
15
20
25
30
35
0
0.5
1
1.5
2
2.5
3

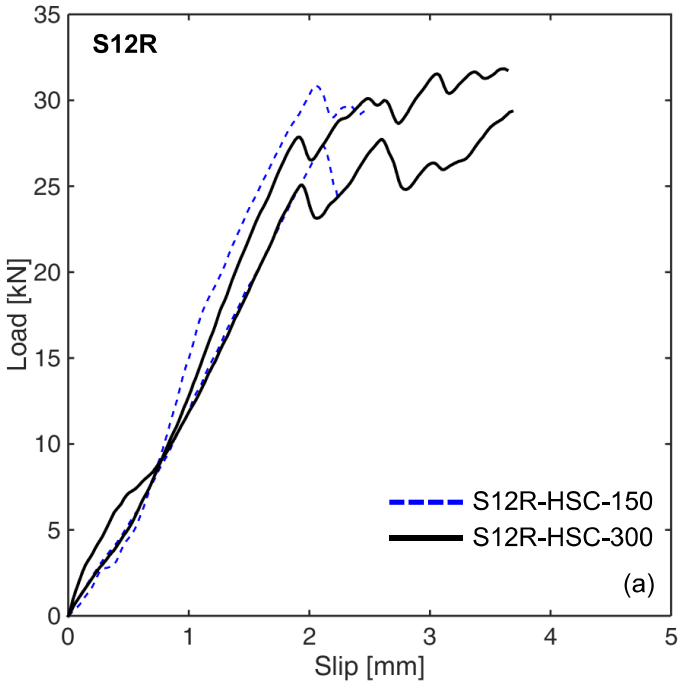
S12R
Load [kN]
Slip [mm]
S12R-HSC-150
S12R-HSC-300
(a)

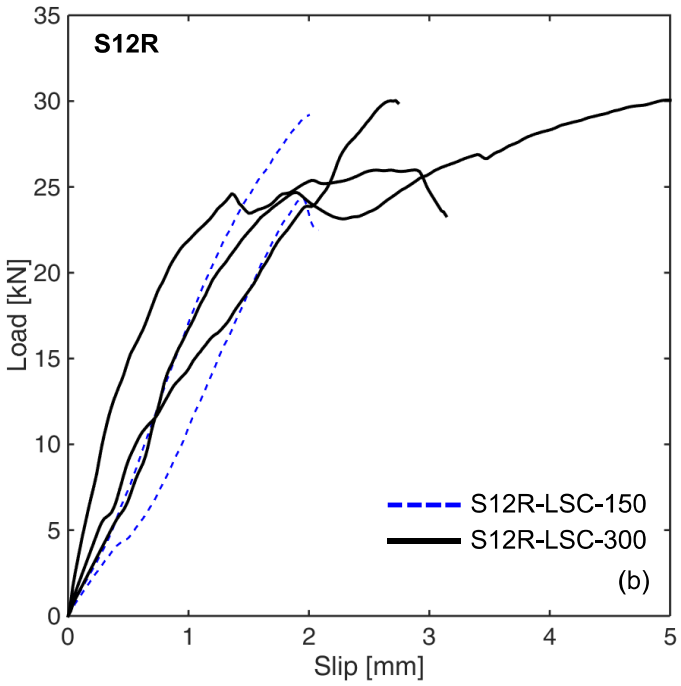
S12R
Load [kN]
Slip [mm]
S12R-LSC-150
S12R-LSC-300
(b)

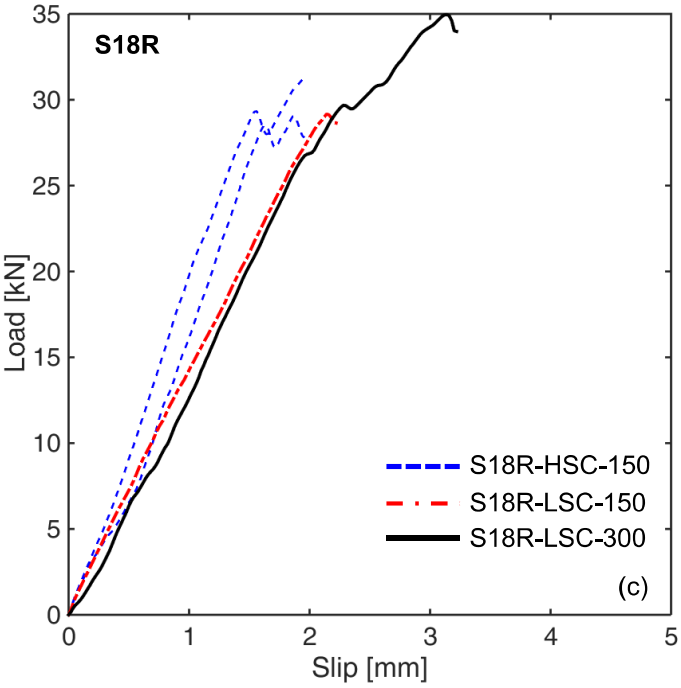
S18R
Load [kN]
Slip [mm]
S18R-HSC-150
S18R-LSC-150
S18R-LSC-300
(c)

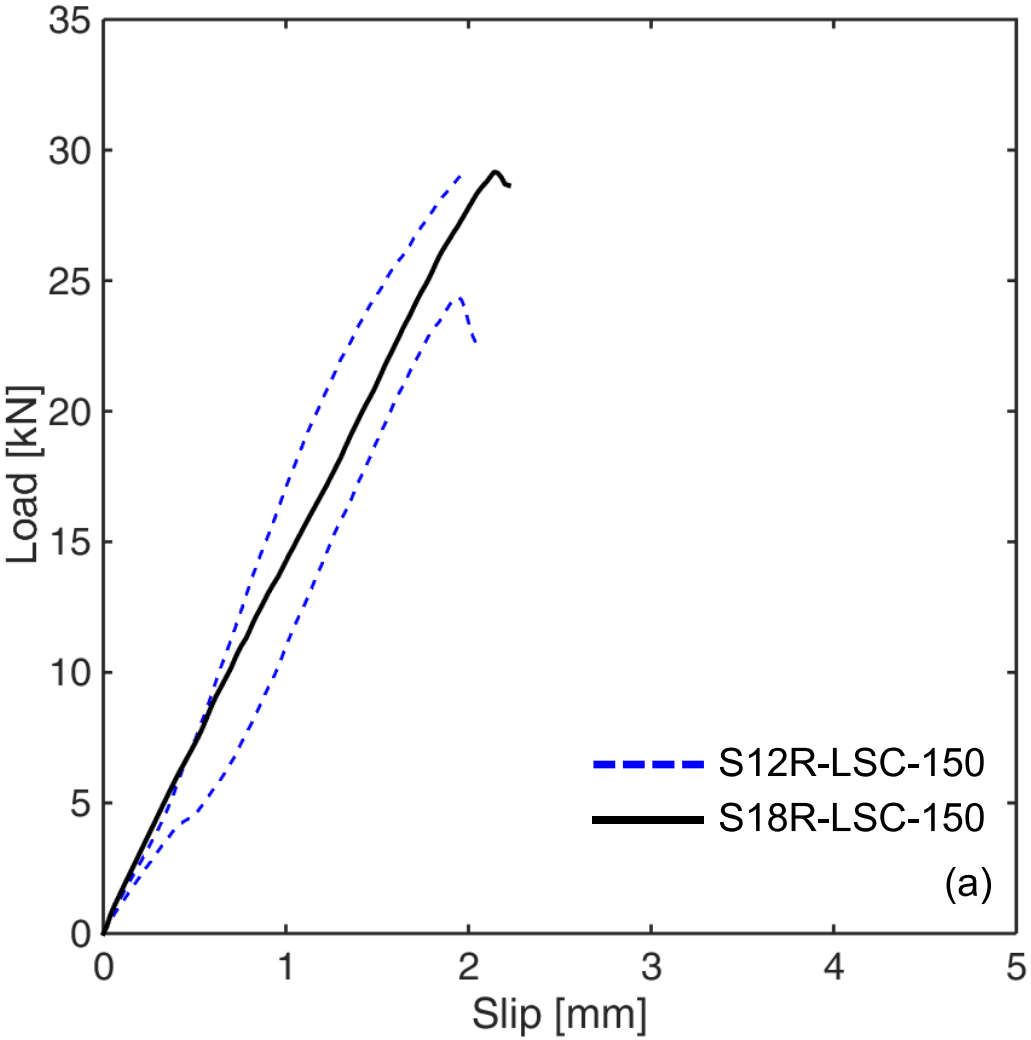
Load [kN]
Slip [mm]
S12R-LSC-150
S18R-LSC-150
(a)

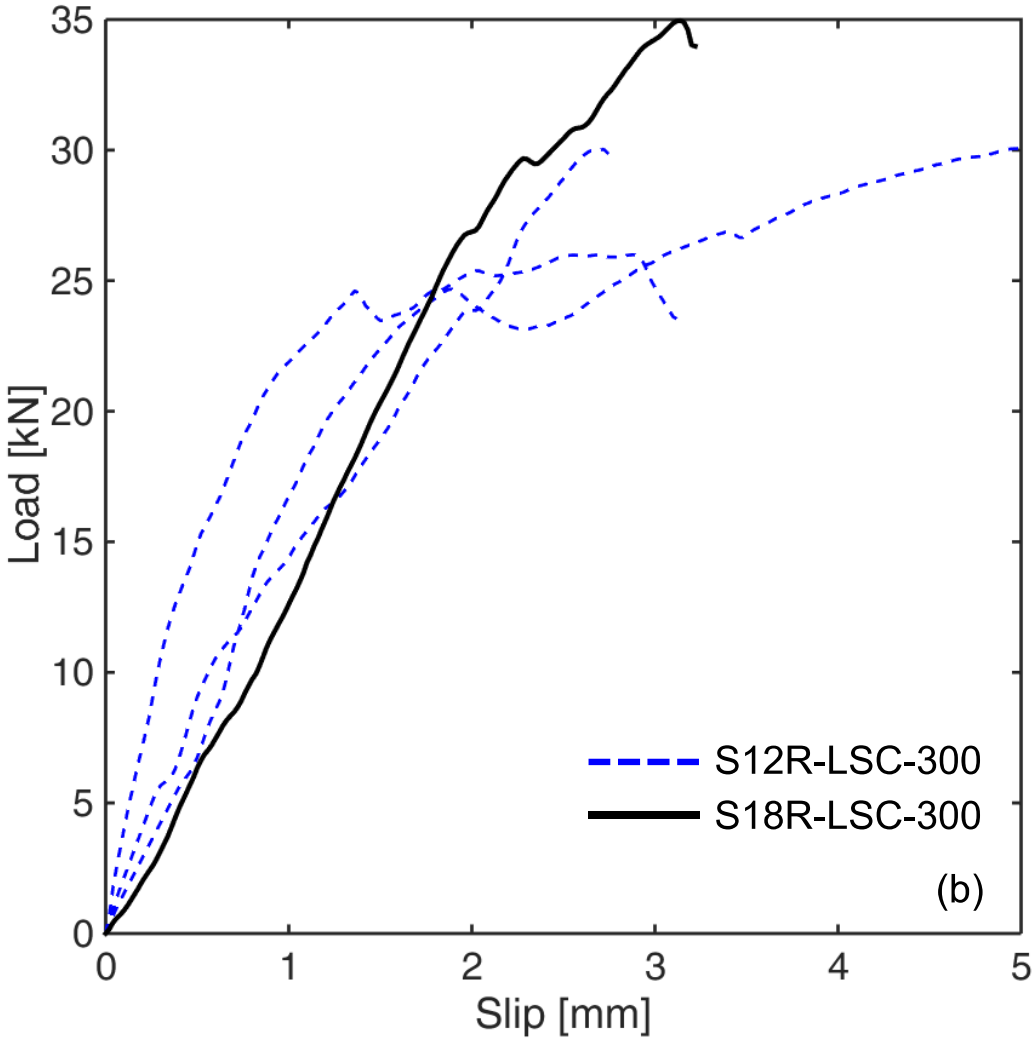
Load [kN]
Slip [mm]
S12R-LSC-300
S18R-LSC-300
(b)


(a)
(b)
(c)
(d)
200
100
50
20
0
mm

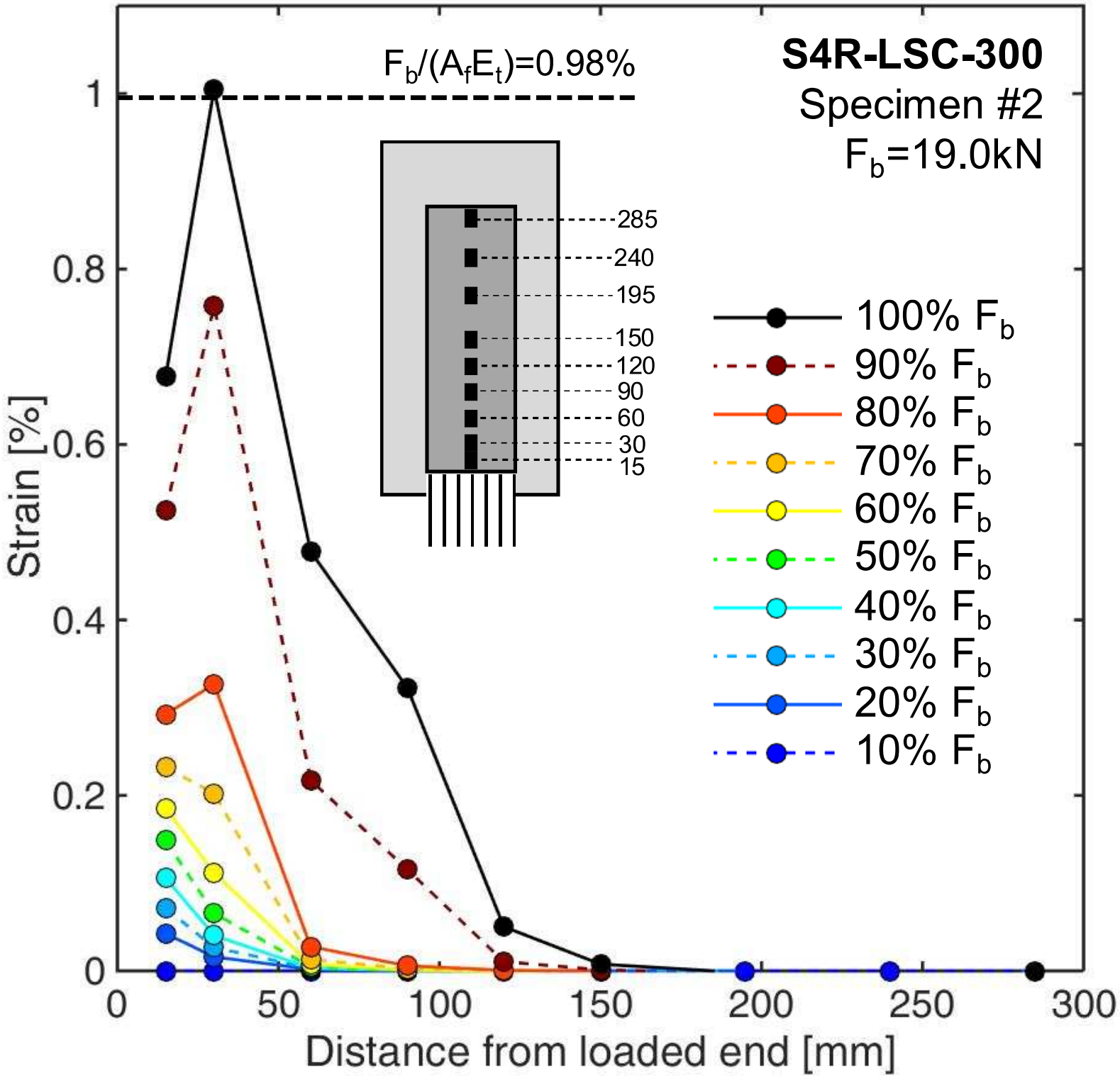
S4R-LSC-300
Specimen #2
F_b=19.0kN
$F_b/(A_fE_t)$=0.98%
285
240
195
150
120
90
60
30
15
100% F_b
90% F_b
80% F_b
70% F_b
60% F_b
50% F_b
40% F_b
30% F_b
20% F_b
10% F_b
Strain [%]
0
0.2
0.4
0.6
0.8
1
0
50
100
150
200
250
300
Distance from loaded end [mm]

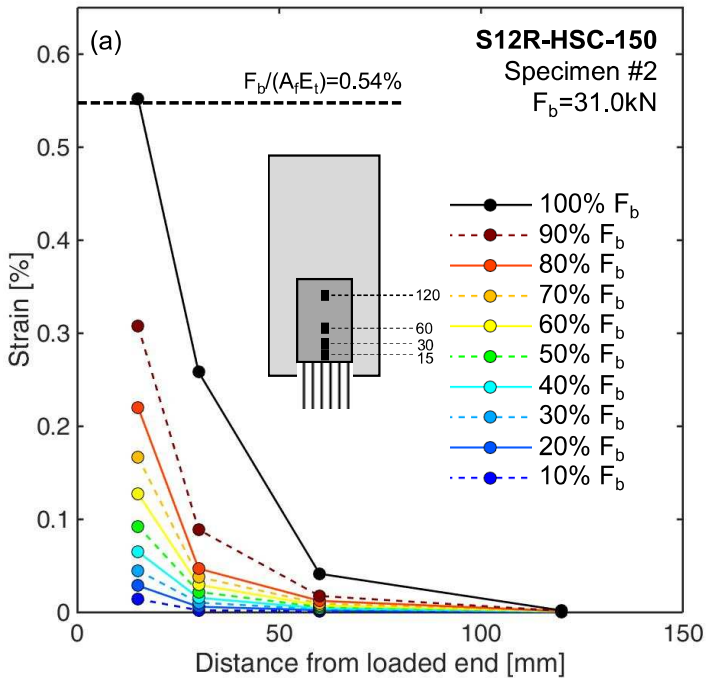
(a)
S12R-HSC-150
Specimen #2
F_b=31.0kN
$F_b/(A_fE_t)$=0.54%
100% F_b
90% F_b
80% F_b
70% F_b
60% F_b
50% F_b
40% F_b
30% F_b
20% F_b
10% F_b
120
60
30
15
Strain [%]
Distance from loaded end [mm]

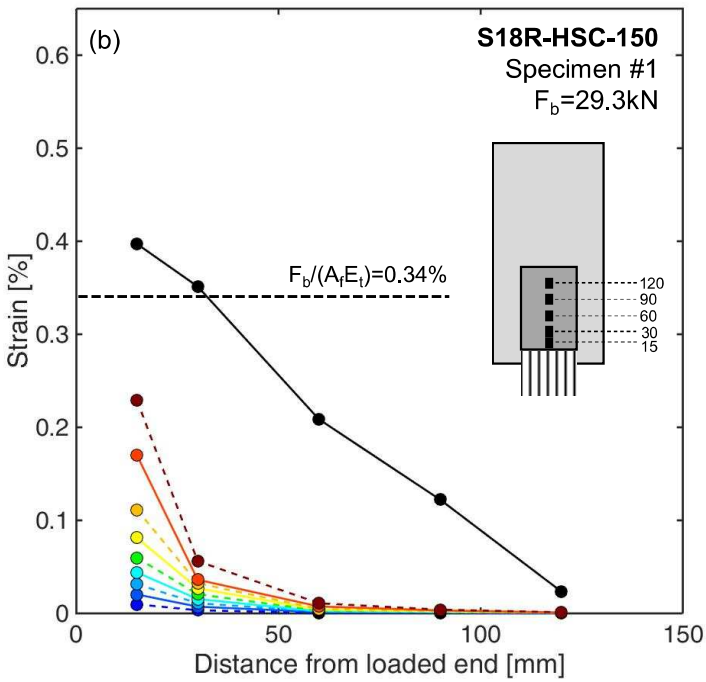
(b)
S18R-HSC-150
Specimen #1
F_b=29.3kN
$F_b/(A_fE_t)$=0.34%
120
90
60
30
15
Strain [%]
Distance from loaded end [mm]

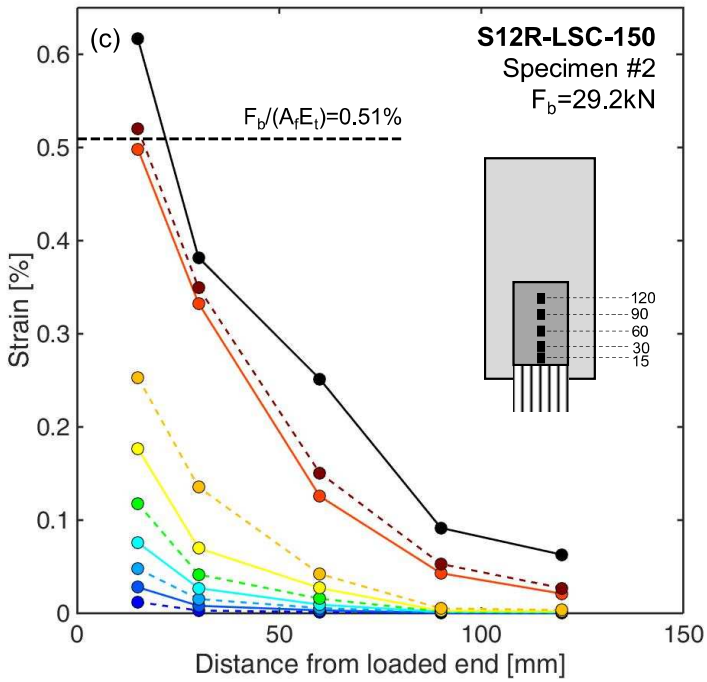
(c)
S12R-LSC-150
Specimen #2
F_b=29.2kN
$F_b/(A_fE_t)$=0.51%
120
90
60
30
15
Strain [%]
Distance from loaded end [mm]

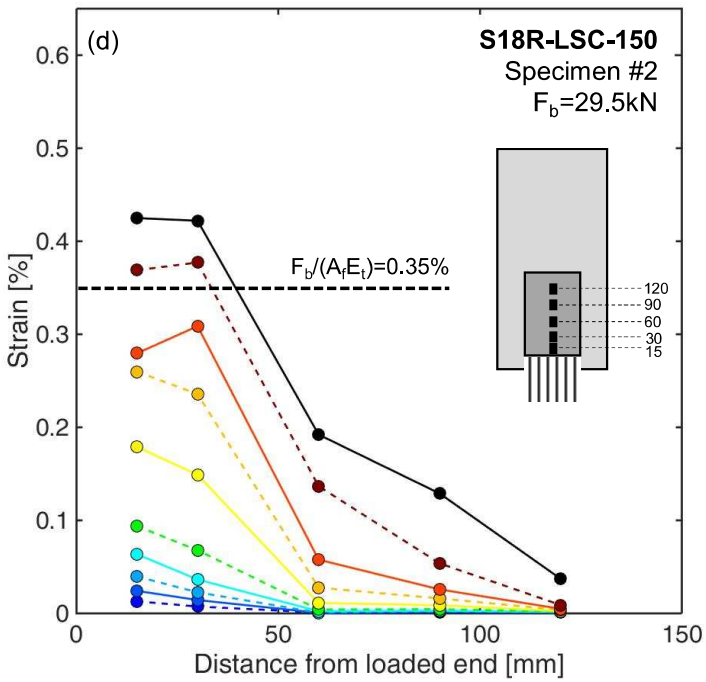
(d)
S18R-LSC-150
Specimen #2
F_b=29.5kN
$F_b/(A_fE_t)$=0.35%
120
90
60
30
15
Strain [%]
Distance from loaded end [mm]

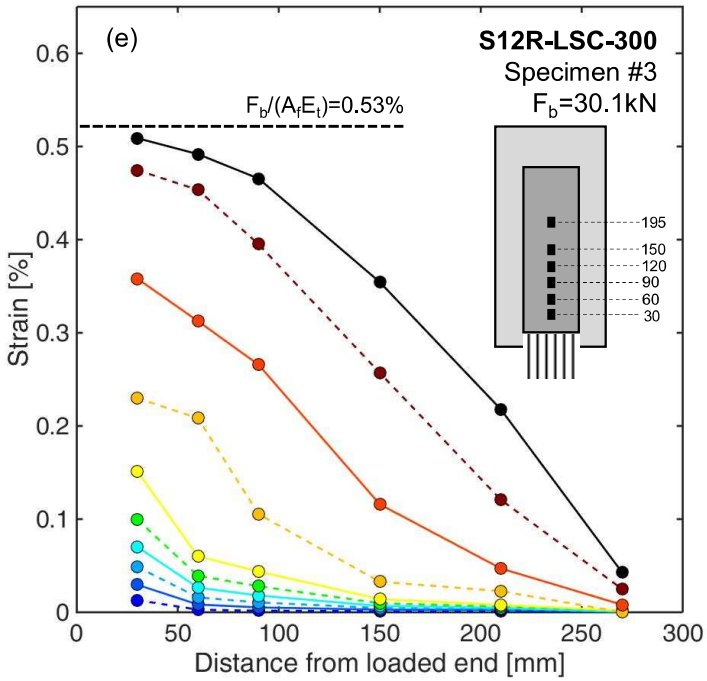
(e)
S12R-LSC-300
Specimen #3
F_b=30.1kN
$F_b/(A_fE_t)$=0.53%
195
150
120
90
60
30
Strain [%]
Distance from loaded end [mm]

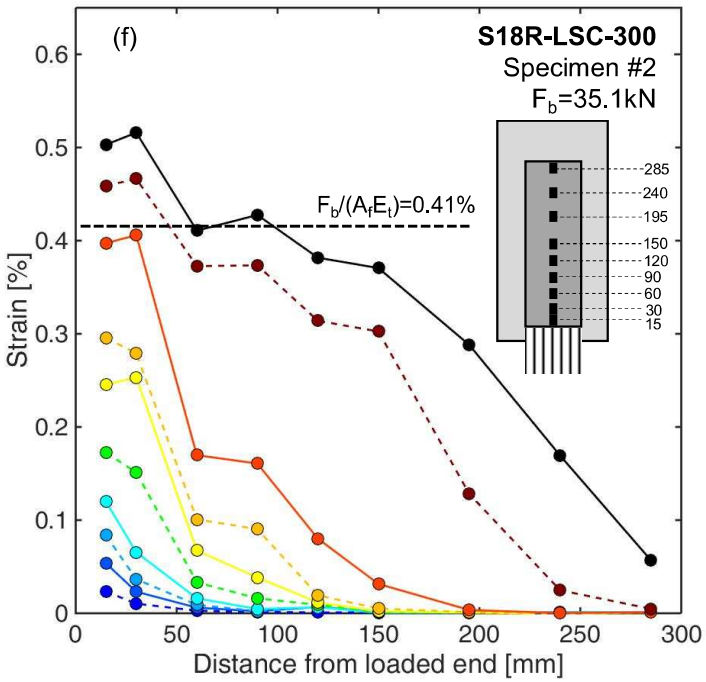
(f)
S18R-LSC-300
Specimen #2
F_b=35.1kN
$F_b/(A_fE_t)$=0.41%
285
240
195
150
120
90
60
30
15
Strain [%]
Distance from loaded end [mm]

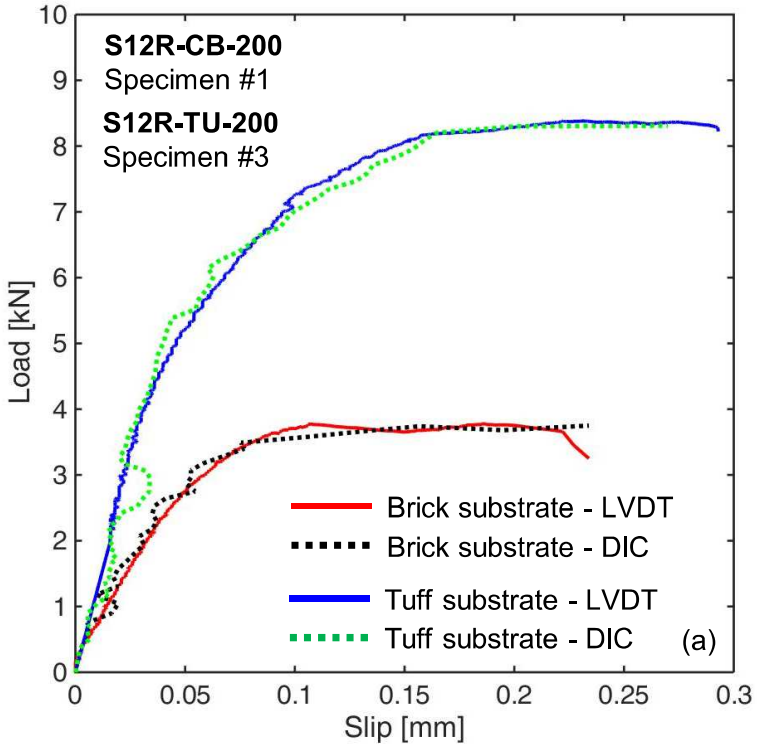
S12R-CB-200
Specimen #1
S12R-TU-200
Specimen #3
Brick substrate - LVDT
Brick substrate - DIC
Tuff substrate - LVDT
Tuff substrate - DIC
(a)
Load [kN]
Slip [mm]

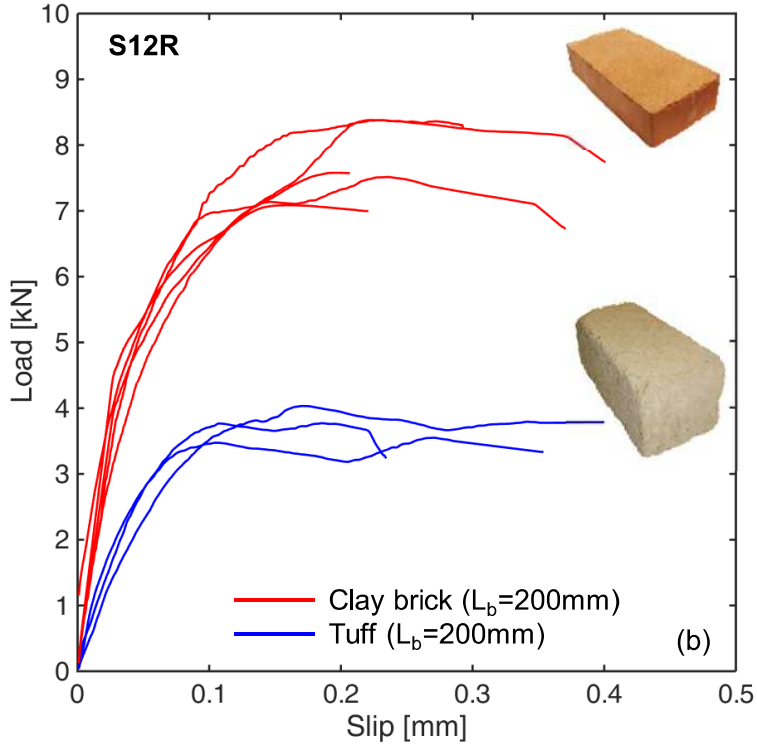
S12R
Clay brick (Lb=200mm)
Tuff (Lb=200mm)
(b)
Load [kN]
Slip [mm]

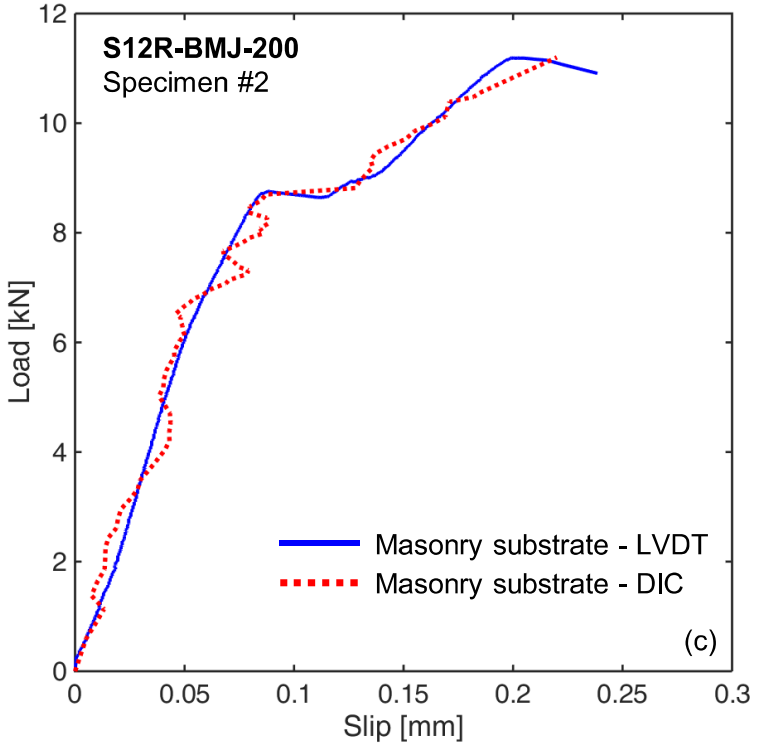
S12R-BMJ-200
Specimen #2
Masonry substrate - LVDT
Masonry substrate - DIC
(c)
Load [kN]
Slip [mm]

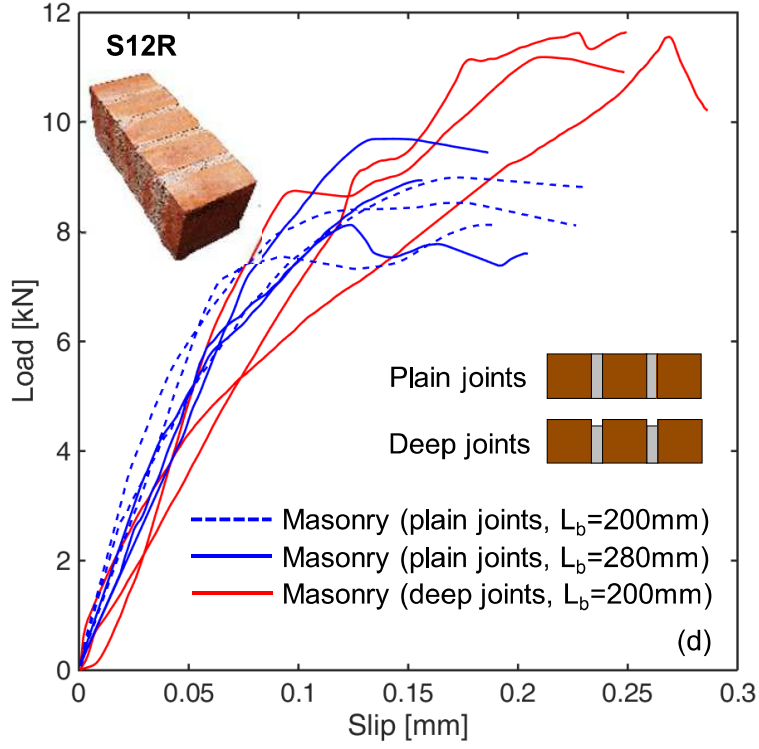
S12R
Plain joints
Deep joints
Masonry (plain joints, Lb=200mm)
Masonry (plain joints, Lb=280mm)
Masonry (deep joints, Lb=200mm)
(d)
Load [kN]
Slip [mm]

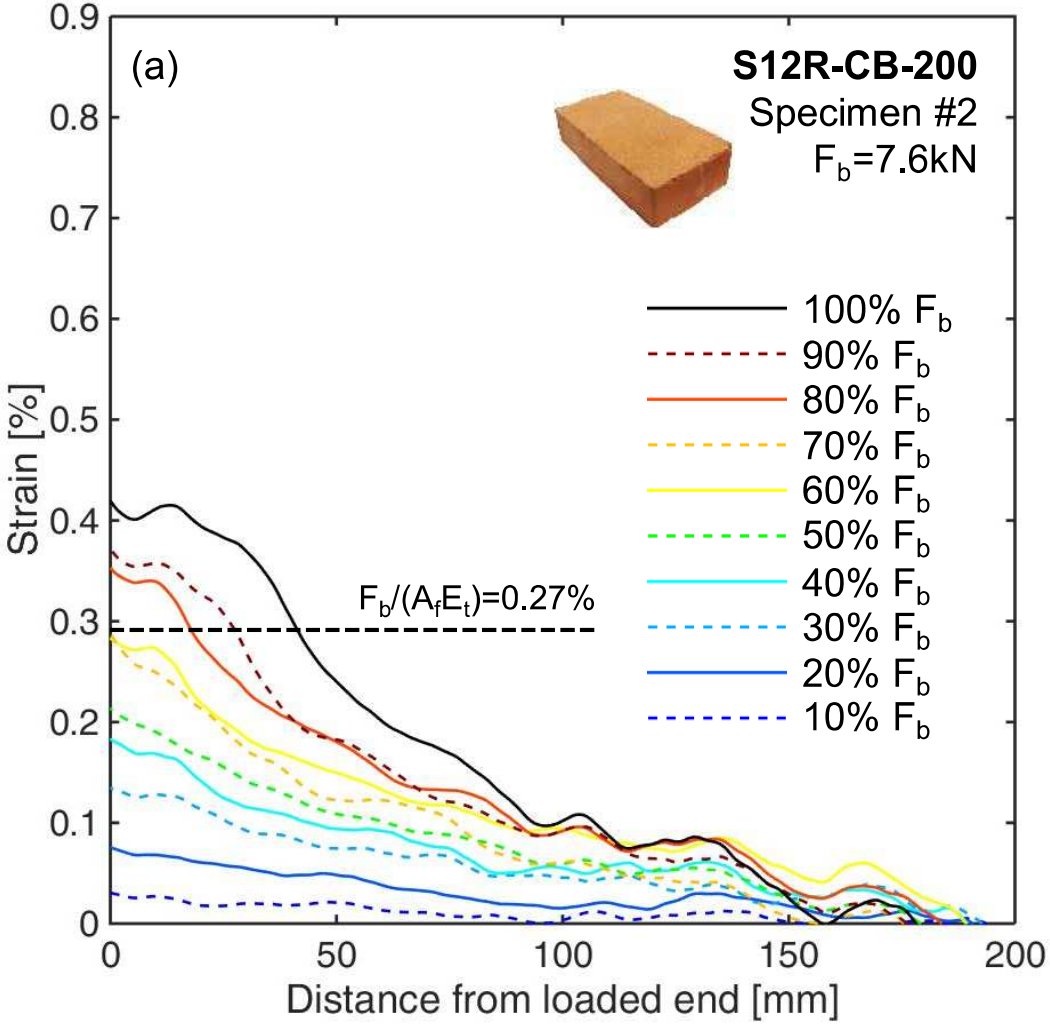
(a)
S12R-CB-200
Specimen #2
F_b=7.6kN
100% F_b
90% F_b
80% F_b
70% F_b
60% F_b
50% F_b
40% F_b
30% F_b
20% F_b
10% F_b
$F_b/(A_fE_t)$=0.27%
Strain [%]
Distance from loaded end [mm]
0
0.1
0.2
0.3
0.4
0.5
0.6
0.7
0.8
0.9
50
100
150
200

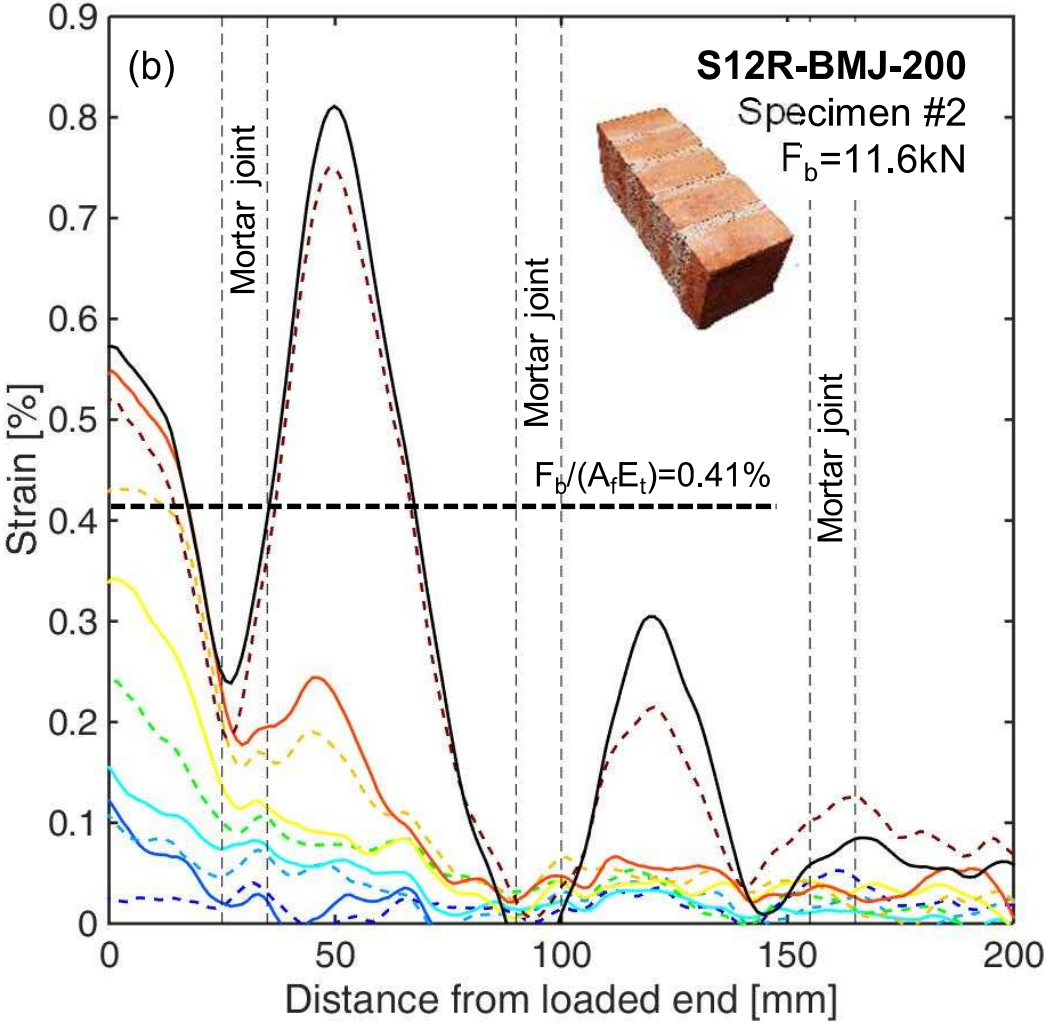
(b)
S12R-BMJ-200
Specimen #2
F_b=11.6kN
Mortar joint
Mortar joint
Mortar joint
$F_b/(A_fE_t)$=0.41%
Strain [%]
Distance from loaded end [mm]
0
0.1
0.2
0.3
0.4
0.5
0.6
0.7
0.8
0.9
50
100
150
200

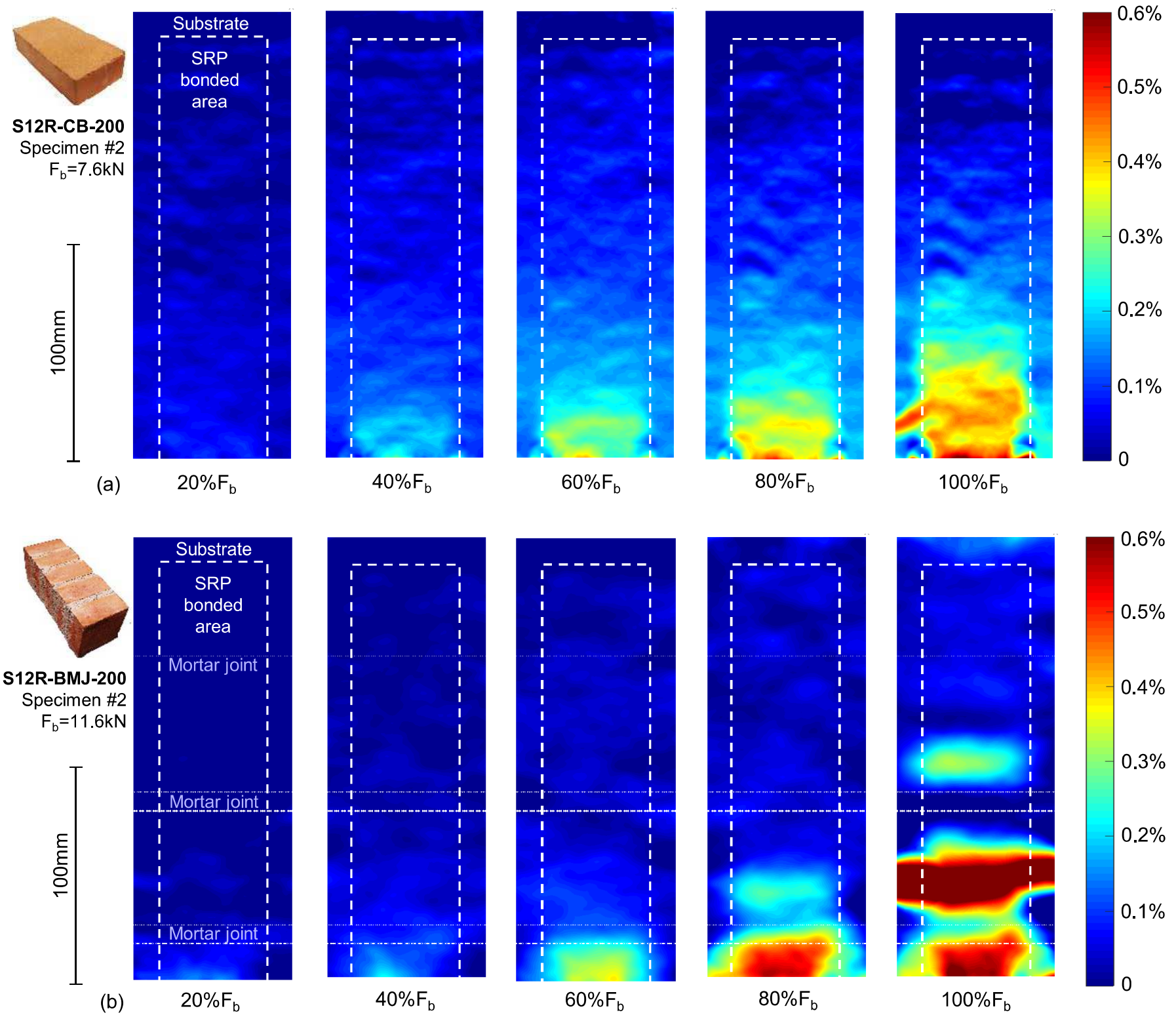
S12R-CB-200
Specimen #2
F_b=7.6kN
Substrate
SRP bonded area
100mm
(a)
20%F_b
40%F_b
60%F_b
80%F_b
100%F_b
0.6%
0.5%
0.4%
0.3%
0.2%
0.1%
0
S12R-BMJ-200
Specimen #2
F_b=11.6kN
Substrate
SRP bonded area
Mortar joint
Mortar joint
Mortar joint
100mm
(b)
20%F_b
40%F_b
60%F_b
80%F_b
100%F_b
0.6%
0.5%
0.4%
0.3%
0.2%
0.1%
0

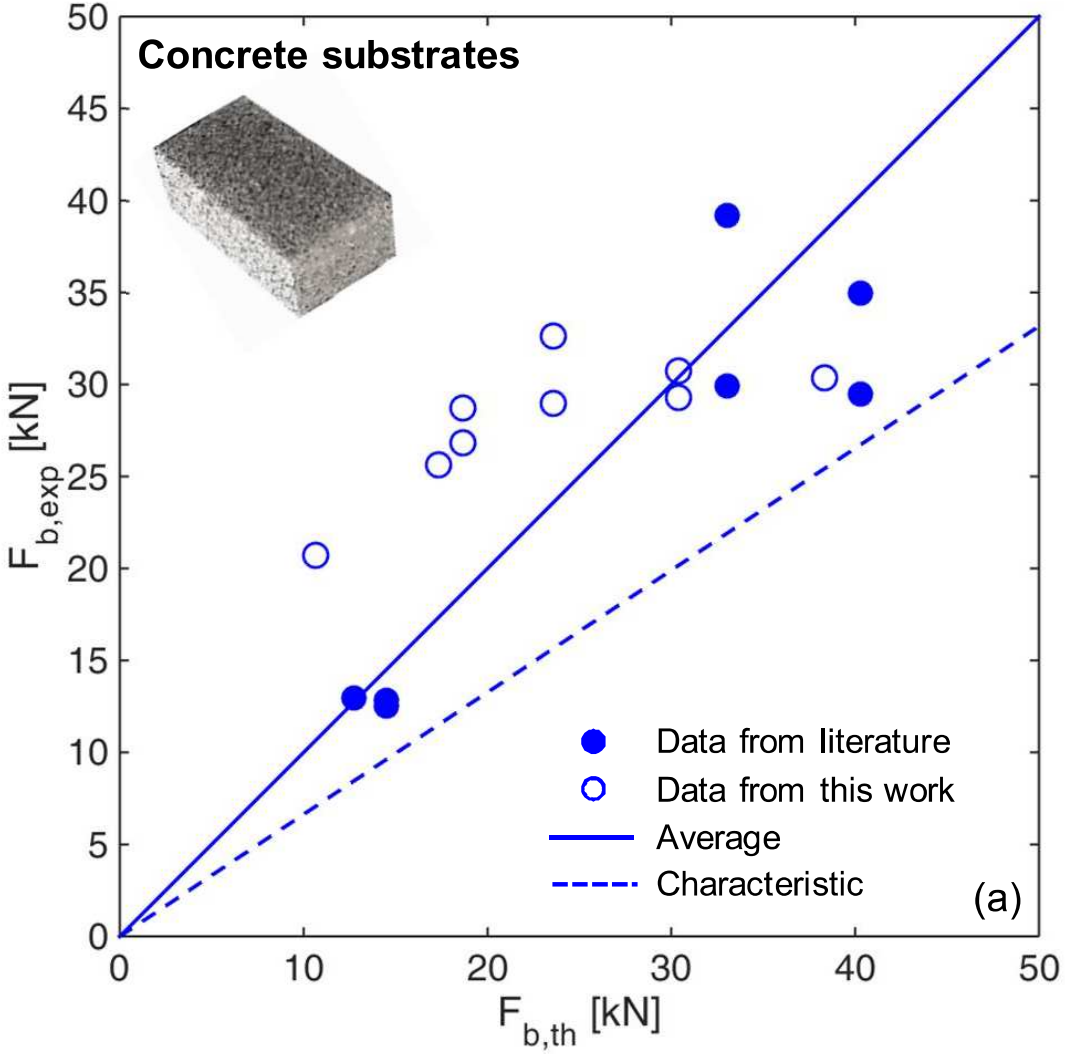
Concrete substrates
$F_{b,exp}$ [kN]
$F_{b,th}$ [kN]
0
5
10
15
20
25
30
35
40
45
50
0
10
20
30
40
50
Data from literature
Data from this work
Average
Characteristic
(a)

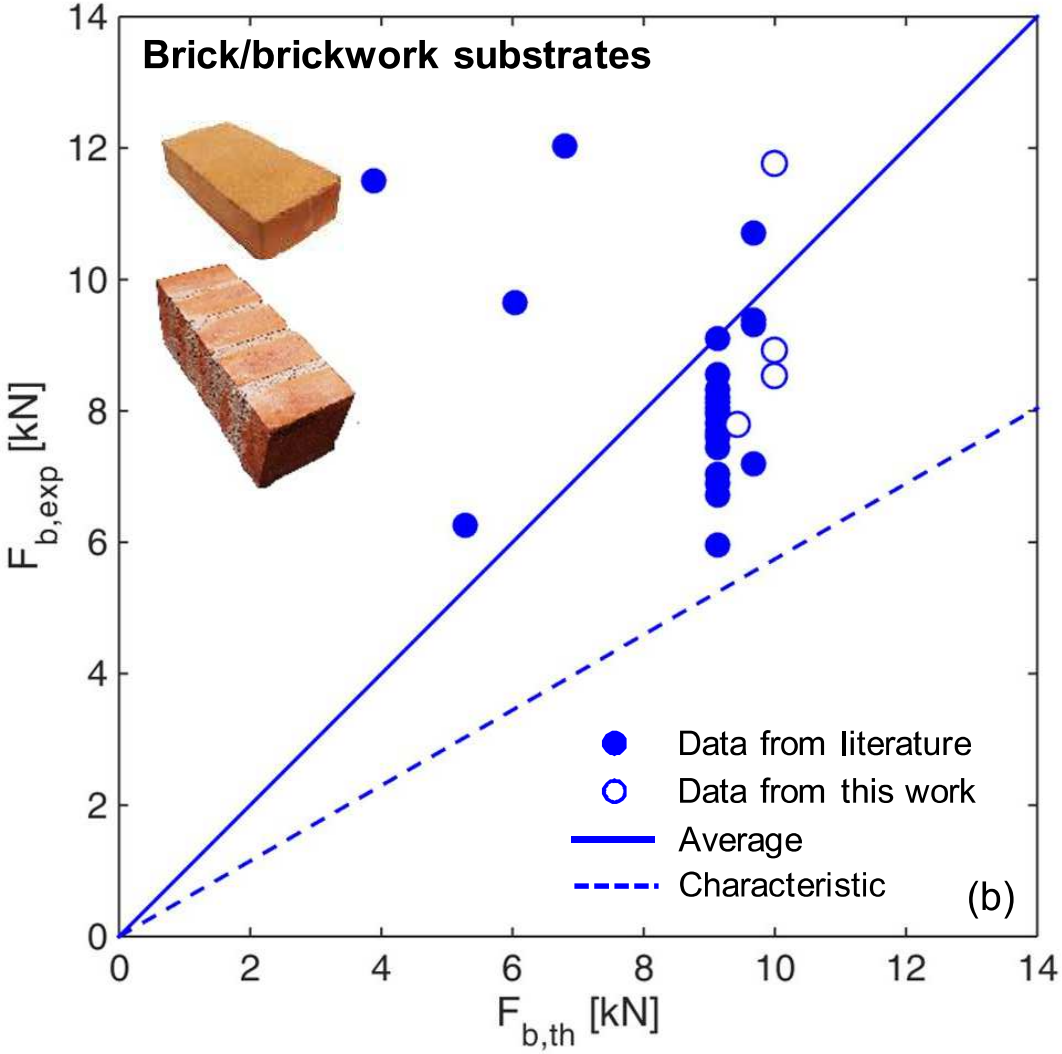
Brick/brickwork substrates
$F_{b,exp}$ [kN]
$F_{b,th}$ [kN]
0
2
4
6
8
10
12
14
0
2
4
6
8
10
12
14
Data from literature
Data from this work
Average
Characteristic
(b)

Table 1

Table 1. Properties of the Ultra High Tensile Strength Steel (UHTSS) textiles.

Steel textile	Density (cord/in)	Density (cords/mm)	Cord spacing (mm)	γ (g/m^2)	t (mm)
S4	4	0.157	6.35	670	0.084
S12	12	0.472	2.12	2000	0.254
S18	18	0.709	1.41	3300	0.381

Table 2

Table 2. Results of tensile tests on dry textile and SRP specimens (CV in round brackets). Five tests were carried out for each series.

Textile/SRP	Series	f_t (N/mm^2)	F_t (kN/m)	E_l (kN/mm^2)	E_t (kN/mm^2)	ε_t (%)
Textile	S4	3191.0 (0.6%)	268.0	–	182.1 (1.4%)	2.19 (0.9%)
SRP	S4R	3289.2 (1.5%)	276.3	369.9 (14.3%)	230.1 (2.6%)	1.89 (1.9%)
Textile	S12	3085.7 (1.0%)	783.8	–	183.4 (2.6%)	2.09 (0.8%)
SRP	S12R	3062.6 (0.6%)	777.9	301.4 (17.9%)	224.2 (6.2%)	1.90 (2.4%)
Textile	S18	3064.6 (0.3%)	1167.4	–	182.2 (4.4%)	2.09 (0.8%)
SRP	S18R	3054.1 (0.8%)	1163.6	264.6 (8.3%)	225.1 (6.9%)	1.95 (1.5%)

Table 3

Table 3. Mechanical properties of the substrates (CV in round brackets).

Type and label	f_{cs} (N/mm^2)	f_{ts} (N/mm^2)	E_{sub} (kN/mm^2)
High strength concrete [HSC]	39.7 (11.5%)	3.04 [(a)]	33.27 [(a)]
Low strength concrete [LSC]	15.2 (4.2%)	1.12 [(a)]	24.94 [(a)]
Tuff unit [TU]	4.4 (13.0%) [(b)]	0.56 (4.5%)	0.78 (10.7%)
Clay brick [CB]	(⊥) 14.8 (8.4%) [(b)] (//) 18.5 (7.2%) [(b)]	1.88 (1.1%)	1.95 (12.0%)
Prism of brick masonry [BM]	8.24 (20.9%) [(c)]	-	2.13 (17.8%) [(c)]

[(a)] Estimated according to Italian Building Code [33]: $f_{ts} = 0.30\ (f_{cs}\text{-}8)^{2/3}$, $E_{cs} = 22000\ (f_{cs}/10)^{0.3}$
[(b)] Normalized strength values [34]
[(c)] [12]

Table 4

Table 4. Results of shear bond tests on concrete substrates (CV in round brackets).

Substrate	Density (cord/in)	L_b (mm)	b_f (mm)	Series	N	$F_{b,i}$ (kN)	s_i (mm)	F_b (kN)	s (mm)	σ_b (N/mm^2)	η (-)	F_b*(kN/m)
High strength concrete	4	300	100	S4R-HSC-300	2	27.24 24.01	*1.82* *1.69*	25.62 (8.9%)	*1.75 (4.9%)*	3050.0	95.6	256.2
	12	150	100	S12R-HSC-150	2	27.60 31.05	2.13 2.07	29.32 (8.3%)	2.10 (2.2%)	1154.3	37.4	293.2
	12	300	100	S12R-HSC-300	2	29.64 31.92	3.70 3.60	30.78 (5.2%)	3.65 (2.0%)	1211.8	39.3	307.8
	18	150	100	S18R-HSC-150	2	29.28 31.42	1.90 1.98	30.35 (5.0%)	1.94 (2.9%)	796.6	22.3	303.5
Low strength concrete	4	300	100	S4R-LSC-300	2	22.38 18.97	– –	20.67 (11.7%)	–	2460.7	77.1	206.7
	12	150	100	S12R-LSC-150	2	24.44 29.20	1.98 1.99	26.82 (12.5%)	1.99 (0.5%)	1055.9	34.2	268.2
	12	300	100	S12R-LSC-300	3	26.05 30.10 30.10	2.91 2.71 –	28.75 (8.1%)	2.81 (4.9%)	1131.9	36.7	287.5
	18	150	100	S18R-LSC-150	2	28.41 29.46	3.25 2.19	28.93 (2.6%)	2.81 (31.4%)	759.3	21.2	289.3
	18	300	100	S18R-LSC-300	2	30.11 35.11	– 3.16	32.61 (10.8%)	3.16 (–)	855.9	23.9	326.1

Table 5

Table 5. Results of shear bond tests on masonry substrates (CV in round brackets).

Substrate	Density (cord/in)	L_b (mm)	b_f (mm)	Series	N	$F_{b,i}$ (kN)	s_i (mm)	F_b (kN)	s (mm)	σ_b (N/mm^2)	η (%)	F_b* (kN/m)
Tuff	12	200	50	S12R-TU-200	3	3.55 4.04 3.78	0.27 0.17 0.11	3.79 (6.5%)	0.18 (44.1%)	298.4	9.7%	54.7
Brick	12	200	50	S12R-CB-200	5	8.38 8.39 7.52 7.09 7.58	0.23 0.23 0.24 0.16 0.20	7.79 (7.4%)	0.21 (15.4%)	603.7	19.6%	132.2
Brick masonry	12	200	50	S12R-BM-200 [(a)]	3	8.13 8.53 8.99	0.17 0.18 0.20	8.55 (5.1%)	0.18 (8.3%)	662.6	21.5%	145.1
	12	280	50	S12R-BM-280 [(a)]	3	8.13 9.70 8.97	0.12 0.14 0.16	8.93 (8.8%)	0.14 (14.3%)	692.2	22.4%	151.6
	12	200	50	S12R-BMJ-200 [(b)]	3	11.65 11.57 11.19	0.23 0.27 0.21	11.47 (2.1%)	0.24 (12.9%)	889.0	28.8%	194.7

[(a)] Plain joints; [(b)] Deep joints

Table 6

Table 6. Database of shear bond tests on concrete substrate.

Reference	N (-)	Substrate properties			SRP properties				Bond strength			
		b (mm)	f_{cs} (N/mm^2)	f_{ts} (N/mm^2)	b_f (mm)	L_b (mm)	t (mm)	E_f (kN/mm^2)	$F_{b,exp}$ (kN)	$\sigma_{b,exp}$ (N/mm^2)	$F_{b,th}$ (kN)	$F_{b,exp}/F_{b,th}$ (%)
Figeys et al., 2005 [4]	1	95	35.0	2.65	95	150	0.601	177.6	29.5	516.7	40.3	73.2%
	2	95	35.0	2.65	95	200	0.601	177.6	35.0	613.0	40.3	86.8%
Manos et al., 2011 [6]	1	250	22.0	2.20	190	–	0.118	210.0	29.9	1333.6	33.0	90.6%
	1	250	22.0	2.20	190	–	0.118	210.0	39.2	1748.4	33.0	118.8%
Matana et al., 2005 [5]	4	191	14.6	1.06	51	203	0.562	179.1	12.8	446.6	14.5	88.3%
	4	191	14.6	1.06	51	305	0.562	179.1	12.5	436.1	14.5	86.2%
Stievanin et al., 2013 [7]	2	145	52.5	4.46	60	250	0.084	190.0	13.0	2579.4	12.9	100.7%
Present study	2	200	15.3	1.13	100	150	0.254	183.4	26.8	1055.1	18.7	143.3%
	2	200	15.3	1.13	100	150	0.381	182.2	29.0	761.2	23.6	122.9%
	2	200	15.3	1.13	100	300	0.084	182.1	20.7	2464.3	10.7	193.5%
	3	200	15.3	1.13	100	300	0.254	183.4	28.7	1129.9	18.7	153.5%
	2	200	15.3	1.13	100	300	0.381	182.2	32.6	855.6	23.6	138.1%
	2	200	39.7	3.04	100	150	0.254	183.4	29.3	1153.5	30.4	96.4%
	2	200	39.7	3.04	100	150	0.381	182.2	30.4	797.9	38.4	79.2%
	2	200	39.7	3.04	100	300	0.084	182.1	25.6	3047.6	17.3	148.0%
	2	200	39.7	3.04	100	300	0.254	183.4	30.8	1212.6	30.4	101.3%

$F_{b,th}$: mean theoretical debonding load for k_G=0.087mm.

Table 7

Table 7. Database of shear bond tests on brick/brickwork substrate.

Reference	N (-)	Substrate properties			SRP properties				Bond strength			
		b (mm)	f_{cs} (N/mm^2)	f_{ts} (N/mm^2)	b_f (mm)	L_b (mm)	t (mm)	E_t (kN/mm^2)	$F_{b,exp}$ (kN)	$\sigma_{b,exp}$ (N/mm^2)	$F_{b,th}$ (kN)	$F_{b,exp}/F_{b,th}$ (%)
Cancelli et al., 2007 [8]	3	120	25.0	2.50	80	0	0.227	190.0	26.8	1475.8	16.4	163.4%
Capozucca, 2010 [9]	3	120	7.3	0.73	50	250	0.097	190.0	11.5	2371.1	3.8	302.6%
de Felice et al., 2015 [12] [(b)]	3	120	14.7	1.88	50	200	0.231	195.1	8.0	692.6	9.1	87.9%
	3	120	14.7	1.88	50	200	0.231	195.1	9.1	787.9	9.1	100.0%
	3	120	14.7	1.88	50	200	0.231	195.1	7.6	658.0	9.1	83.5%
	3[(a)]	120	18.5	1.88	50	195	0.231	195.1	9.3	805.2	9.6	96.9%
	3[(a)]	120	18.5	1.88	50	195	0.231	195.1	10.7	926.4	9.6	111.5%
	3[(a)]	120	18.5	1.88	50	195	0.231	195.1	7.2	623.4	9.6	75.0%
	3[(a)]	120	18.5	1.88	50	200	0.231	195.1	9.4	813.9	9.6	97.9%
Grande et al., 2011 [10]	5	120	45.3	4.53	25	160	0.227	190.0	12.0	2114.5	7.8	153.8%
	3	120	35.6	3.56	25	160	0.227	190.0	9.6	1691.6	6.9	139.1%
	5	120	27.2	2.72	25	160	0.227	190.0	6.3	1110.1	6.0	105.0%
Valluzzi et al., 2012 [11] [(b)]	5	120	14.7	1.88	50	160	0.231	195.1	6.7	580.1	9.1	73.6%
	5	120	14.7	1.88	50	160	0.231	195.1	7.7	666.7	9.1	84.6%
	5	120	14.7	1.88	50	160	0.231	195.1	7.8	675.3	9.1	85.7%
	4	120	14.7	1.88	50	160	0.231	195.1	7.4	640.7	9.1	81.3%
	5	120	14.7	1.88	50	160	0.231	195.1	8.3	718.6	9.1	91.2%
	3	120	14.7	1.88	50	160	0.231	195.1	8.1	701.3	9.1	89.0%
	5	120	14.7	1.88	50	160	0.231	195.1	8.6	744.6	9.1	94.5%
	5	120	14.7	1.88	50	160	0.231	195.1	7.0	606.1	9.1	76.9%
	1	120	14.7	1.88	50	160	0.231	195.1	8.2	710.0	9.1	90.1%
	5	120	14.7	1.88	50	160	0.231	195.1	7.0	606.1	9.1	76.9%
	5	120	14.7	1.88	50	160	0.231	195.1	8.0	692.6	9.1	87.9%
	5	120	14.7	1.88	50	160	0.231	195.1	8.0	692.6	9.1	87.9%
	5	120	14.7	1.88	50	160	0.231	195.1	7.6	658.0	9.1	83.5%
	5	120	14.7	1.88	50	160	0.231	195.1	6.0	519.5	9.1	65.9%
Present study	5	120	14.7	1.88	50	200	0.254	183.4	7.8	614.2	9.4	83.0%
	3[(a)]	120	18.5	1.88	50	200	0.254	183.4	11.8	929.1	10.0	118.0%
	3[(a)]	120	18.5	1.88	50	200	0.254	183.4	8.5	669.3	10.0	85.0%
	3[(a)]	120	18.5	1.88	50	280	0.254	183.4	8.9	700.8	10.0	89.0%

$F_{b,th}$: mean theoretical debonding load for k_G=0.052mm.

[(a)] Tests on brick masonry substrate.
[(b)] Round Robin Test (RRT) programs. Tests carried out by different laboratories were grouped in different datasets.